Artificial Intelligence In Medicine 130 (2022) 102331

Contents lists available at ScienceDirect

Artificial Intelligence In Medicine

journal homepage: www.elsevier.com/locate/artmed

Deep learning for image-based liver analysis — A comprehensive review focusing on malignant lesions

Shanmugapriya Survarachakan [a,*], Pravda Jith Ray Prasad [b,c], Rabia Naseem [d], Javier Pérez de Frutos [e], Rahul Prasanna Kumar [b], Thomas Langø [e], Faouzi Alaya Cheikh [d], Ole Jakob Elle [b,c], Frank Lindseth [a]

[a] Department of Computer Science, Norwegian University of Science and Technology, 7491 Trondheim, Norway
[b] The Intervention Centre, Oslo University Hospital, 0372 Oslo, Norway
[c] Department of Informatics, University of Oslo, 0315 Oslo, Norway
[d] Department of Computer Science, Norwegian University of Science and Technology, 2815 Gjøvik, Norway
[e] Department of Health Research, SINTEF A.S., 7030 Trondheim, Norway

ARTICLE INFO

Keywords:
Deep-learning
Liver
Lesions
Hepatic vessels
Segmentation

ABSTRACT

Deep learning-based methods, in particular, convolutional neural networks and fully convolutional networks are now widely used in the medical image analysis domain. The scope of this review focuses on the analysis using deep learning of focal liver lesions, with a special interest in hepatocellular carcinoma and metastatic cancer; and structures like the parenchyma or the vascular system. Here, we address several neural network architectures used for analyzing the anatomical structures and lesions in the liver from various imaging modalities such as computed tomography, magnetic resonance imaging and ultrasound. Image analysis tasks like segmentation, object detection and classification for the liver, liver vessels and liver lesions are discussed. Based on the qualitative search, 91 papers were filtered out for the survey, including journal publications and conference proceedings. The papers reviewed in this work are grouped into eight categories based on the methodologies used. By comparing the evaluation metrics, hybrid models performed better for both the liver and the lesion segmentation tasks, ensemble classifiers performed better for the vessel segmentation tasks and combined approach performed better for both the lesion classification and detection tasks. The performance was measured based on the Dice score for the segmentation, and accuracy for the classification and detection tasks, which are the most commonly used metrics.

1. Introduction

Liver cancer is the sixth most frequently diagnosed cancer and the third most frequent cause of cancer death worldwide [1]. Hepatocellular carcinoma (HCC) is a primary tumor occurring in the liver and comprises a diverse group of cancer varying genetically as well as molecularly and accounting for 70 % to 85 % of the total liver cancer burden worldwide [2]. Cancer in the liver can also be secondary cancer due to metastasis of other primary tumors e.g., from colorectum, breast or pancreas. In terms of clinical outcomes, variations in the liver tumor subclasses are significant. In post-operative control, the tissue architecture also differs significantly, which leads to alteration in vascular supply and surge in cellularity. This variation in tissue architecture of the liver delivers a root for non-invasive detection of liver tumors in imaging despite variable structures and shapes [3]. The irregular shape and texture of the liver and its lesions in the medical images are initial biomarkers of hepatic tumor disease diagnosis. Both computed tomography (CT) and magnetic resonance imaging (MRI) are well suited to detect vessel structures and lesions and are used by surgeons for surgical planning. Intraoperative ultrasound (US) imaging is used to detect lesion depth and position for precise resection by sparing as much healthy liver volume as possible (parenchyma sparing technique).

Precise segmentation and classification are of utmost importance in computer-aided diagnosis, treatment planning, surgical guidance and post-operative surveillance (Fig. 1). Especially in pre-operative plannings, precise segmentation and classification of the lesions can lead to a smaller resection margin, hence sparing more tissue. However, due to artifacts in liver images such as heterogeneity in the intensity

* Corresponding author.
E-mail address: shanmugapriya.survarachakan@ntnu.no (S. Survarachakan).

https://doi.org/10.1016/j.artmed.2022.102331
Received 23 July 2021; Received in revised form 23 May 2022; Accepted 30 May 2022
Available online 9 June 2022

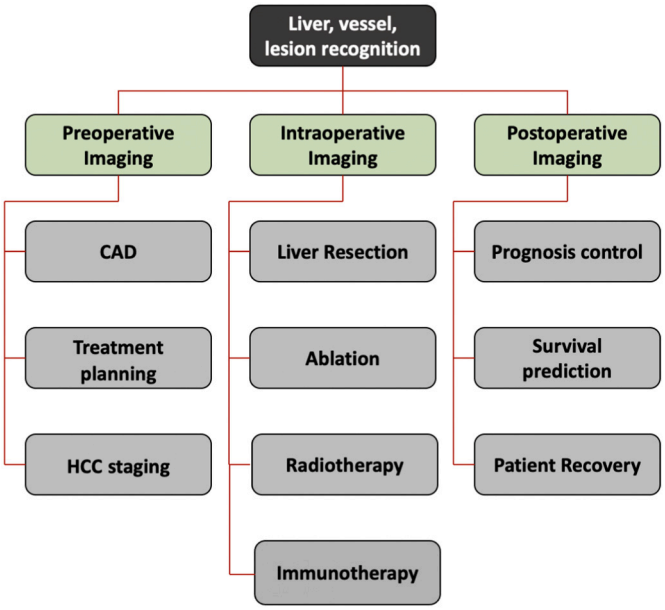

Fig. 1. Role of liver image analysis.

information within the liver, varying shape, low contrast between liver parenchyma and lesions, weak boundaries between liver and other abdominal organs; automatic segmentation of liver, liver vessels, and lesions becomes challenging. In addition, due to varying acquisition protocols, different contrast agents, varying scanner resolution and different enhancement techniques; robust and automatic segmentation and classification of liver parenchyma, vessels, and lesions still remains an open challenge and has recently attracted considerable research attention.

In clinical practice, manual and semi-automatic methods are used by radiologists to detect, delineate and classify the lesions and other structures in medical images. These methods are time-consuming, operator-dependent and cost-ineffective. In the past, various deterministic and probabilistic approaches have been proposed to achieve accurate segmentation and analysis of the liver, its vessels, and also quantification of liver fat from different medical images [4–9]. Other extensively studied methods include region growing, active contour, level set, graph cuts, clustering and methods based on thresholding, deformable models, statistical shape models, sigmoid edge modeling and learning-based approaches like Support Vector Machine (SVM) [10–15].

Associated with the Medical Image Computing and Computer-Assisted Intervention (MICCAI) conference in 2007 [16] and 2008 [17], two grand challenges were conducted to segment liver and lesions. The majority of the works presented in these two challenges were based on traditional approaches. However, a new trend could be observed in the 2017 edition of the Liver Tumor Segmentation challenge (LiTS) of MICCAI [18], where a great majority of submitted works were based on deep learning (DL) and machine learning methods, reporting higher accuracy than the previous challenges. Recent studies have shown the diverse application of DL based liver image analysis [19–26]. In this paper, we present a comprehensive review of recent methods for automatic detection, segmentation and classification of liver parenchyma, liver vessels and liver lesions using DL.

Our contribution: In this work, the state-of-the-art in DL-based detection, segmentation and classification of liver, vessels and lesions with a focus on malignant liver tumors is presented. In total, 91 papers are reviewed, summarized (Fig. 7) and categorized based on the methodology (Section 8). The top three methods for each of the five tasks (liver segmentation, lesion segmentation, vessel segmentation, lesion classification and lesion detection) are ranked based on the DICE score for segmentation and accuracy for classification and detection tasks. The best performing DL architectures/methodology, data handling and research lines are discussed.

The literature review performed for the present work is based on a structured search for articles in the databases Google Scholar, Web of Science, PubMed, Oria, Research Gate, research books and conference proceedings using the keywords “liver”, “liver lesion”, “liver vessels”, “deep learning”, “segmentation”, “detection” and “classification”. The review articles are excluded and the last update to the included papers was on February 15, 2022.

The present review paper is organized in such a way that Sections 2 to 7 give a general introduction to the anatomy of the liver, imaging techniques for liver lesion diagnostics, image analysis tasks, artificial neural network architectures, challenge datasets and evaluation metrics for liver image analysis. Then Section 8 deals with the review of the selected articles, followed by the discussion in Section 9, list of future research lines in Section 10, and conclusion in Section 11.

2. Anatomy and function of the liver

The liver is both the largest internal organ and the largest gland in the human body. Hepatocytes, bile canaliculi and hepatic sinusoids are the main components of the liver. Being the most common cell type, the hepatocytes form close to 80 % of the liver [27]. The hepatocytes and sinusoids form the lobules, which are considered the functional unit of this organ [28]. The liver is positioned in the upper right part of the abdomen. It has multiple vital roles including vital metabolism, glycogen storage regulation, detoxification of drugs, red blood cells decomposition and hormone production. The liver also produces bile, which helps in the breakdown of fat. The hepatic vascular system comprises the hepatic artery, the hepatic vein and the portal vein. The hepatic artery carries blood from the aorta to the liver, the hepatic vein drains deoxygenated blood from the liver into the inferior venacava, and the portal vein carries blood containing the digested nutrients from the gastrointestinal tract, spleen and pancreas to the liver [27].

The liver has four lobes known as left, right, caudate and quadrate. Based on Couinaud classification [30], the liver is divided into eight functionally independent segments, each of them having its own vascular inflow, outflow and lymph drainage, as shown in Fig. 2. According to Bismuth [31], Segment IV is sometimes divided into segments

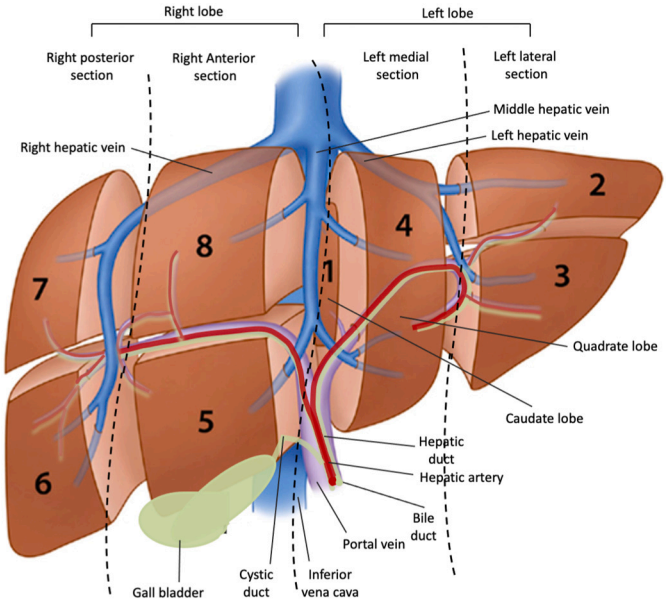

Fig. 2. Anatomy of liver.
Adapted from Orcutt et al. [29].

IVa and IVb. Segment I is located posteriorly and it is not visible in the frontal view. The periphery of each segment has a vascular outflow through the hepatic veins. The middle hepatic vein partitions the liver into the right and left lobes. The right hepatic vein partitions the right lobe into anterior and posterior segments. The falciform ligament partitions the left lobe into a medial part consisting of Segment IV, and a lateral part consisting of segments II and III. The portal vein divides the liver into upper and lower segments.

Readers interested in more details about the liver are referred to Betts et al. [27]; Lorente et al. [28].

3. Imaging techniques for liver lesion diagnostics

Medical imaging enables the detection, characterization and diagnosis of tumorous masses in the organ. It is less traumatic than a biopsy [32] and provides a quick and reliable way for doctors to analyze the lesion. Especially in HCC, imaging aims to detect the presence of metastasis. CT, MRI and US are the most used imaging modalities for liver lesions [33–37]. Out of these, CT and MRI are the preferred modalities for screening, detection and characterization, because of higher specificity and sensitivity [33,35,36,38]. That is, diagnosis based on CT and MRI images, with better resolution and level of detail than US, present a higher precision when discerning healthy and non-healthy patients, and identifying ailments. Despite ionizing radiation exposure, CT and more specifically contrast-CT [36], remains the preferred modality due to its low cost, short scanning time, and highly detailed images [33,37].

In this context, special attention should be given to multiphase CT angiography, where images are acquired before, during and after the administration of contrast agents, allowing the detection of changes in blood supply and the possibility to study the hemodynamics of the liver tumor (Fig. 3). Unlike conventional CT angiography, in multiphase CT angiography, the images are acquired during a specific arterial interval.

With the advancements in CT techniques such as dynamic multidetector CT, Volume Perfusion CT (VPCT), Dual Energy CT (DECT) and Cone Beam CT (CBCT); high-resolution images can be acquired easing the diagnosis and staging of HCC. The majority of the studies analysed in this review use CT images.

On the other hand, MRI provides a better characterization of small lesions ($\leq$3 cm) than CT, and so it is used as a supplementary modality to the former [37]. However, its complexity and long acquisition times make it inadequate for routine examinations. In Europe, between 2013 and 2018, the average increase in the number of acquisitions has been 14.48 per 1000 people. In T2-weighted imaging, the lesion tissue is hyperintense or isointense compared to the surrounding parenchyma. Therefore, to characterize liver lesions, T2-weighted imaging alone is not always sufficient because it can be isointense in some cases. On the other hand, on T1-weighted images liver lesion tissue is mostly hypointense. However, lesions smaller than 1.5 cm tends to be isointense in T1-weighted images. Examples of T1 and T2 weighted, as well as Diffusion-Weighted MRI images, are shown in Fig. 4.

Diffusion-Weighted MRI (DW-MRI) provides insight information about the tumor viability at the cellular level and is well suited to differentiate HCC from dysplastic nodules [39]. However, contrast-enhanced MRI (CE-MRI) outperforms DW-MRI in the detection and characterization of HCC. Dynamic Contrast-Enhanced MRI (DCE-MRI) improves the detection of blood vessels in tissues, thus is well suited for the assessment of HCC lesions since these lesions are highly vascularized. A combination of DW-MRI and CE-MRI shows improved performance in the detection of HCC tissue in chronic liver diseases [40]. In addition, MR spectroscopy and MR elastography are used for detection, staging and differentiation between benign and malignant liver lesions. Besides HCC, MRI has been found to be effective in characterizing different types of benign and malignant FLLs. For instance, several research works report dynamic gadolinium-enhanced MRI to perform best in this regard Zhang et al. [41]. Long Time to Echo (TE) T2 MRI is very accurate in discriminating haemangiomas from solid lesions, whereas DWI precisely classified 89.5 % malignant and 88 % benign lesions.

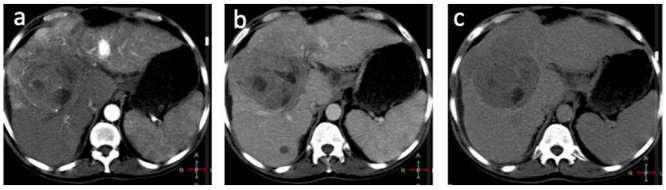

Fig. 3. CT of metastatic malignancy a) arterial phase b) portal venous phase c) delayed phase. Case courtesy of Dr. Ahmed Abdrabou, Radiopaedia.org, rID: 22888. https://radiopaedia.org/cases/22888.

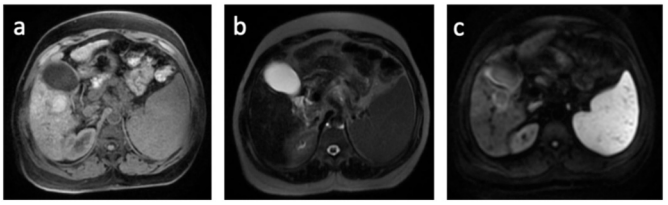

Fig. 4. MRI of metastatic malignancy a) T1-weighted unenhanced b) T2-weighted c) DW-MRI. Case courtesy of Dr. Mohammad A. ElBeialy, Radiopaedia.org, rID: 28994. https://radiopaedia.org/cases/28994.

US provides a cheap and reliable method for a routine examination, which can be performed as often as required [33]. US is a radiation-free modality often suitable for children, pregnant women and patients recommended to go through repetitive diagnostic scanning. Nonetheless, the use of this modality highly depends on the experience of the user, as well as the interpretation of the images, unlike CT or MRI [33]. Contrast-enhanced US (CEUS) has been shown to provide a better characterization of the lesion, especially small tumor masses [33,42]. CEUS uses microbubbles as the contrast agent. These are administered into the intravascular space, which is soon cleared from the blood pool and moved into the extracellular space [43]. The diagnosis of liver tumors based on CEUS is carried out using arterial phase hypervascularity and portal or delayed phase washout.

In CEUS, the scanning of the entire liver is not possible and it is less sensitive to diagnose small lesions, compared to the aforementioned imaging modalities. In addition, CEUS image interpretation is highly dependent on the experience of the operator, has a limited field of view and the body characteristics of patients can limit the visualization of the entire liver in the contrast phase. So, CEUS is used to characterize the previously identified liver lesions and can be used as a supporting diagnostic tool (Fig. 5). Furthermore, US elastography [44] and Acoustic

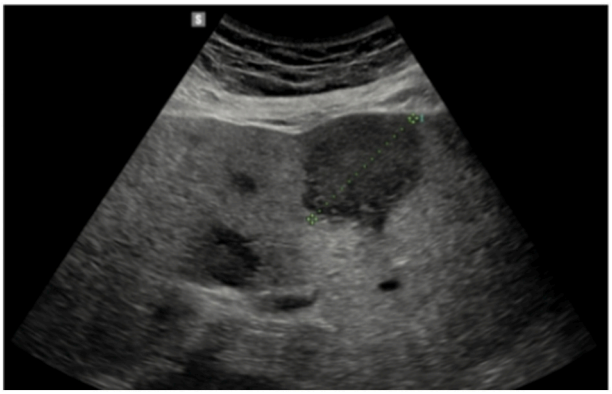

Fig. 5. CEUS of metastatic malignancy. Case courtesy of Dr. Balint Botz, Radiopaedia.org, rID: 70877. https://radiopaedia.org/cases/70877.

Radiation Force Impulse [45] are new US technologies used to study the characteristics of biological tissue, which helps to differentiate benign and malignant lesions. US elastography is being used for quantitative evaluation of liver stiffness. Besides, image analysis on US variants shows promising performance to study diffuse liver diseases, monitoring steatosis staging, fatty liver staging yielding moderate to high sensitivity [20,46–49]. CEUS is frequently integrated with locoablative therapies to determine the response of the treatment.

The intraoperative US is of high value for intraoperative navigation in minimally invasive surgery. This modality enables the examination of the organ during the intervention to locate the lesions and relevant structures [50,51]. The increase in interest in minimally invasive surgery comes hand-to-hand with the introduction of navigation platforms in the operating room (OR), and thus, an increase in the use of intraoperative modalities. Furthermore, hybrid ORs bring together radiologists and surgeons as it allows the use of intraoperative CT scanners as well as MRI scanners in the surgical workflow [52]. This market is expected to grow in the next years, increasing the use of CT images in liver surgery, for examination and navigation, as well as laparoscopic US for navigation [50,51]. Also, with the rise of ablation as a treatment for smaller lesions [53,54], the use of intraoperative modalities like CT or US, for the location of lesions, needle placement, and evaluation of the ablation, can be expected to increase in the coming years.

The following trends were observed regarding the use of CT and MRI. The use of US was not reported, the authors understand the use of US is widely extended and used in routine examinations. In Europe, the number of abdominal CT scans has doubled in the span of seven years, from 2008 to 2015; from 14.4 to 28.9 procedures per 1000 population [55,56]. And in a broader scope, in Europe, there has been an average increase in the number of CT scans of 25.15 $\pm$ 20.75 per 1000 inhabitants between 2013 and 2018 [57]. In this same time span, the number of MRI scans has increased on average 14.48 $\pm$ 13.51 per 1000 inhabitants [57]. Regarding these same technologies, countries of the Organisation for Economic Co-operation and Development (OECD) reported an increase of 53.2 CT acquisitions per 1000 inhabitants in the span of 2007 to 2017 [58]. In this same time span, the number of MRI scans increased by 31.3 per 1000 inhabitants [58]. Hence, there is a preference in the use of CT as a primary examination tool, leaving MRI as a supplementary modality together with US [36,37,59].

4. Image analysis tasks

Analysis and interpretation of images involve four main tasks, which have been traditionally called classification, localization, detection and segmentation (Fig. 6). Despite this distinction, image analysis applications are usually implemented in a combined fashion, making it difficult to sort them into one of these four categories. Classification is the process of identifying the class or label to which the object in the image belongs to. In liver image analysis, classification tasks are generally focused on classifying the liver from other organs, classifying the liver tissue as a lesion or healthy, or classifying lesions as benign or malignant. Image classification is often combined with localization, which is defined as the process of finding the coordinates of the desired object in the image. The object localization task returns a bounding box that circumscribes the location of the main object in the image. In some medical image analysis tasks, localization is used as a preliminary step for more complex tasks like segmentation. By identifying the area most likely to contain the desired anatomical structure, and thus, reducing the search space, the computational complexity and processing time of these latter tasks can be improved. Detection is the process of determining all the target objects in the image, that can be of multiple categories, typically identified by bounding boxes and associated labels. Object detection aims at finding anomalies from medical or pathological images and can also be used for tracking purposes. Segmentation is the most important and complex part of medical image analysis, as it focuses on detecting the boundaries of the object (liver, vessels, tumor) either

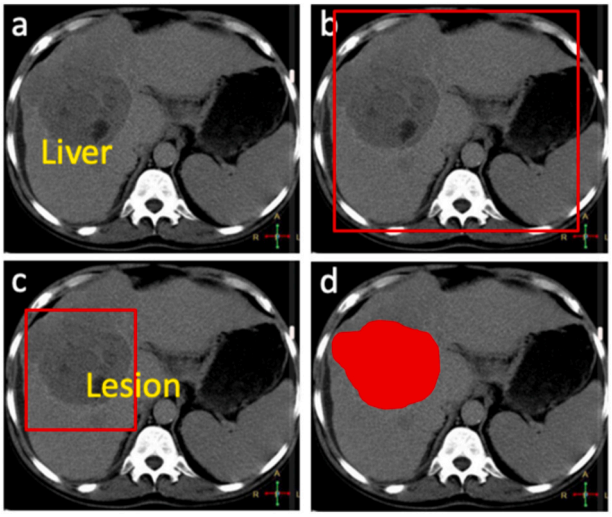

Fig. 6. Liver/lesion recognition task. a) Liver image classification b) Liver localization c) Liver lesion detection d) Liver lesion segmentation. Case courtesy of Dr. Ahmed Abdrabou, Radiopaedia.org, rID: 22888.

automatically, semi-automatically, or manually within 2D or 3D medical data. To do so, the segmentation algorithm maps each pixel to its rightful class i.e. the correct type of tissue or organ. There are two types of segmentation namely semantic and instance segmentation. Semantic segmentation assigns the same label to all pixels/objects of the same class (e.g. lesion) whereas instance segmentation provides a unique label to each object of a given class (e.g. lesion number 1, lesion number 2). That is, it differentiates between instances of the same label. In liver resection surgery and radiotherapy treatment, reliable segmentation guides the radiologists to treat the diseased part, sparing as much healthy tissue as possible.

5. Artificial neural networks

Artificial Neural Networks (ANN) are inspired by the human nervous system. Like the human brain, ANNs are composed of several individual processing units called artificial neurons [60]. These units are interconnected in a similar way as biological neurons through axons, which transmit information between the neurons. In the nervous system, this information is coded in electric-chemical impulses, while in ANNs it is in the numerical value returned by the activation function of the neuron that is passed on. The activation function operates over the weighted sum of all the inputs to the neuron. The weights together with a bias factor are the learnable parameters of the neuron.

In ANNs, neurons are arranged in layers. Stacking several of these layers result in a Multi-Layered Perceptron (MLP). The generic architecture comprises an input layer, several hidden layers and an output layer. The training observations or inputs are fed through the input layer. The hidden layers learn and encode the relationships and patterns in the data, by adjusting the input weights of the neurons. The result of the hidden layers is then passed on to the output layer which formats the output according to the given task e.g. numerical for regression tasks, or probabilities for classification tasks.

There are three different types of learning schemes for ANN i.e., supervised, unsupervised and reinforcement learning. Supervised learning is a task-driven method. It is normally used for classification or regression tasks, based on historical data. In supervised learning, the network is trained by providing the input data along with the corresponding correct output or ground truth. This way, the parameters of the ANN (weights and biases) are iteratively tuned based on the difference between the prediction and the ground truth. Backward propagation (backpropagation) training falls within this category of training

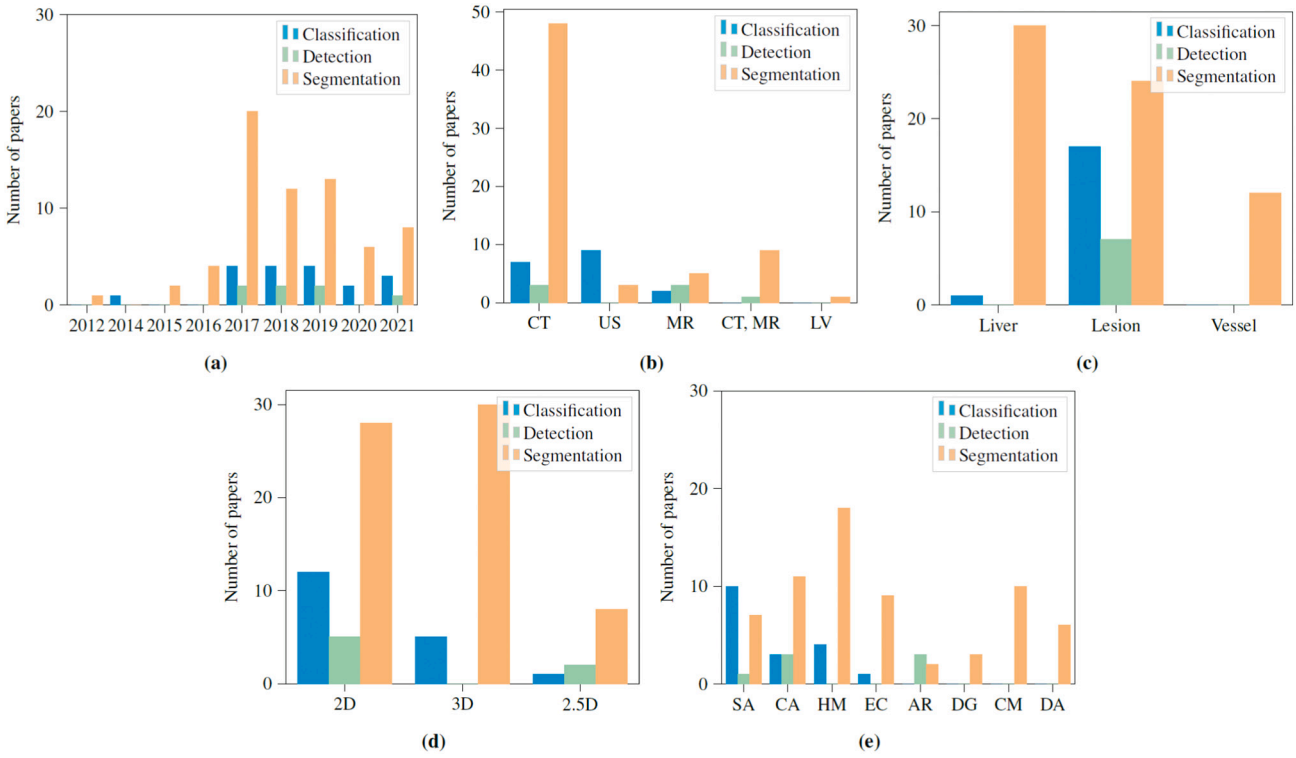

Fig. 7. Applications of deep learning in liver image analysis. (a) Year of the publication; (b) modality (LV - laparoscopic videos); (c) ROI - Region of interest; (d) dimensionality; (e) methodology (SA - single-step approach or end-to-end learning, CA - combined approach, HM - hybrid model, EC - ensembled classifier, AR - atlas registration, DG - detection guidance, CM - cascaded model, DA - domain adaptation) (Section 8).

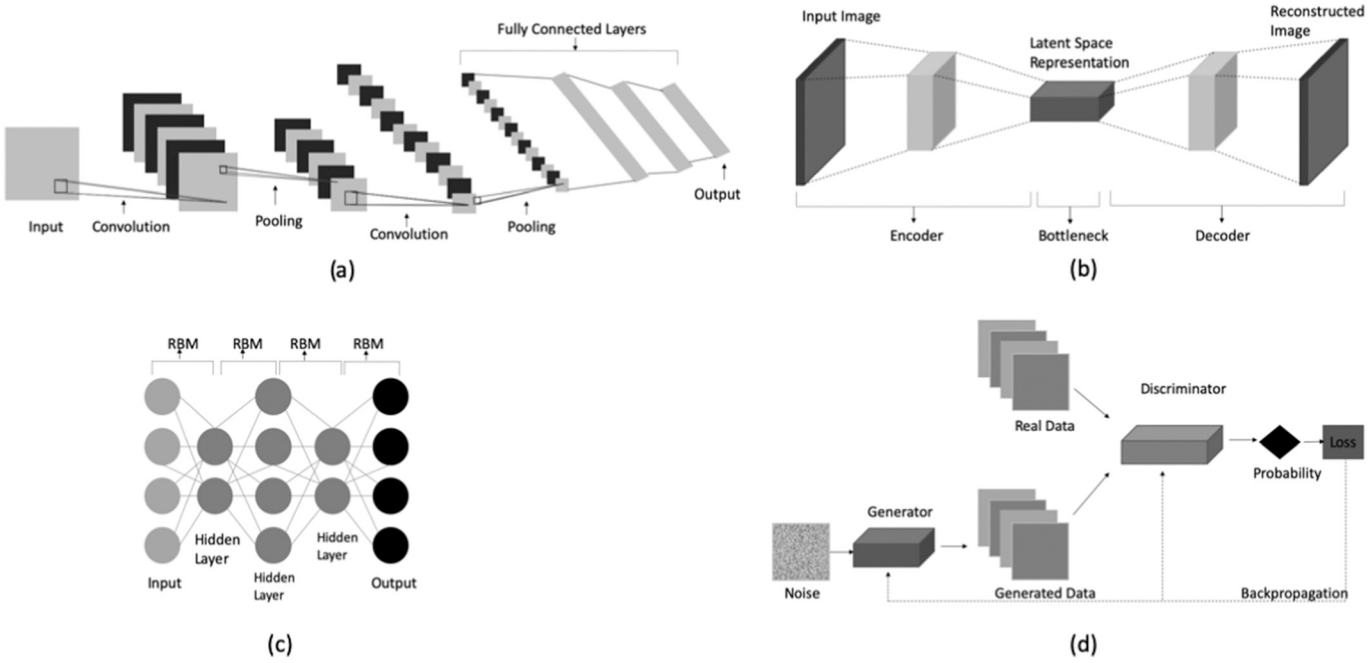

Fig. 8. ANN Architectures a) Convolutional Neural Network, b) Autoencoder, c)Deep Belief Network, d) Generative Adversarial Network.

methods. Related to supervised training a new strategy named semi-supervised learning has gained momentum recently. This is also data-driven, but unlike supervised training, the ground truth is not available. Instead, the output is evaluated based on a priori information on the expected output [26]. Unsupervised learning is a data-driven method used to train descriptive models for a given dataset, where no a priori target is provided and all features are equally important. These ANNs are generally used for clustering problems. Reinforcement learning differs from supervised learning in which the former involves learning by interacting with the environment.

Though there are many ANN architectures, the following designs (Fig. 8) have been proved to be very powerful for solving liver imaging

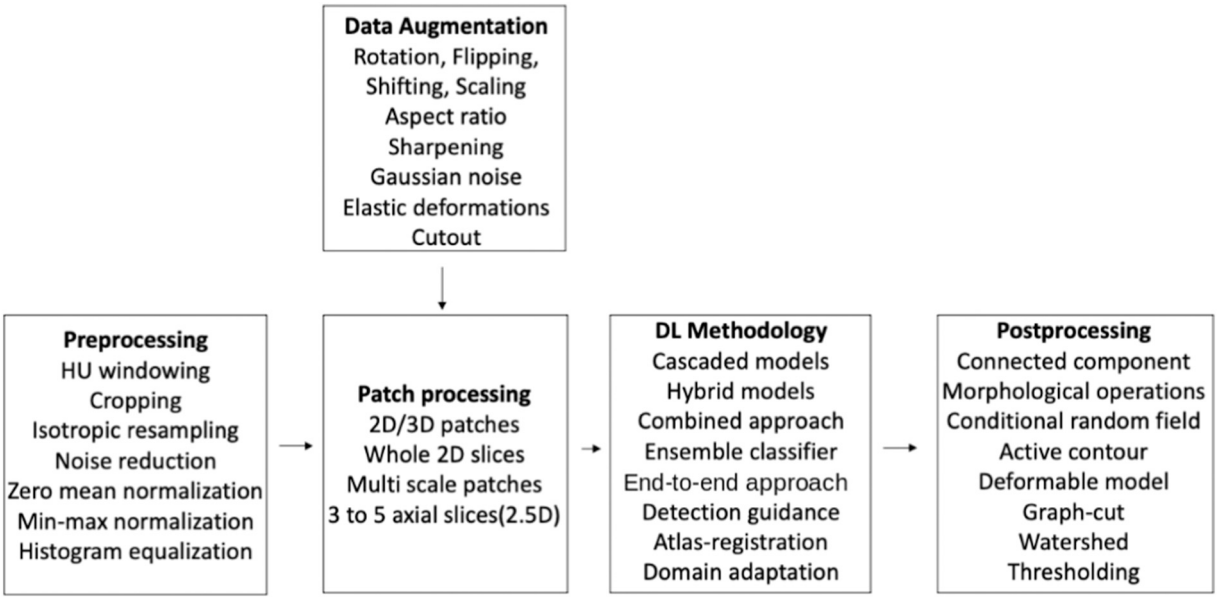

Fig. 9. Summary of the preprocessing, patch processing, DL methodology and post-processing methods used in the papers reviewed.

related tasks.

5.1. Convolutional neural network

Convolutional Neural Networks (CNN) LeCun et al. [61]; Lecun et al. [62] are architecture composed of convolutional layers, which are responsible for detecting certain local features throughout the input images. The convolutional layers comprise a set of stacked filters, each composed of neurons, which generate a unique activation or feature map of the input. Each neuron takes a subregion of the input image as input, which can overlap until the whole image is sampled. Unlike MLPs, each neuron or perceptron in the filter is connected to its neighboring neurons, sharing the input weights. This allows the neurons to react to the same local features throughout the input channels. Each set of shared weights are known as kernels or convolutional kernels. Thus, a convolutional layer with N convolutional kernels produces N feature maps by learning to detect N local features. Each sequence of convolutional layers is typically followed by a pooling layer, which reduces the size of the feature maps by selecting and combining features from the overlapping or non-overlapping local neighborhoods. For example, max-pooling layers select the features with the highest response level, and can further improve translation invariance. A CNN consists of several pairs of convolutional and pooling layers followed by several fully connected layers or MLP, and a softmax layer or regression layer as the output layer to generate the desired outputs. This way, the set of convolutional and pooling layers becomes the equivalent of the feature extractor step in more classic approaches, while the MLP relates to the classification step.

5.2. Auto encoders

Autoencoders (AEs) are unsupervised ANNs that efficiently learn how to compress and encode the data, and then reconstruct the compressed data back to a representation similar to the original input [63]. AEs generally consist of three main parts namely: encoder, bottleneck, decoder. The encoder learns how to reduce and compress the input data into the encoded representation. The bottleneck is the hidden layer that contains the compressed representation which is the smallest possible representation of the input data. The decoder learns to reconstruct the encoded representation of the input data to be as close to the original data as possible. The similarity between the original data and the reconstruction is evaluated during training by the reconstruction loss. To minimize the reconstruction loss the backpropagation method is used during training. The ideal AE model should be sensitive enough to accurately build a reconstruction, and insensitive enough to memorize or overfit the training data. This tradeoff holds the model to maintain only the variations in the data required to reconstruct the input data while ignoring the noise. Due to dimensionality reduction, the AEs can be regarded as a more powerful generalization of principal component analysis (PCA).

The PCA tries to discover a lower-dimensional hyperplane that best describes the original data and the AEs are accomplished in learning non-linear manifolds. Deep autoencoders are a type of AEs typically consisting of a large number of layers for both the encoder and decoder.

5.3. Deep belief networks

Deep Belief Networks (DBN) are probabilistic generative models composed of multiple layers of stochastic and latent variables [64]. The latent variables are often called hidden units or feature detectors and they typically have binary values. The hidden units represent features that captures the correlation present in the input data. DBN is a stack of Restricted Boltzmann Machines (RBM) or AEs. The top two layers are undirected, have symmetric connections between them and form an associative memory. The connections between all the lower layers are directed acyclic connections that convert the associative memory into observed variables. The states of the units in the lowest layer represent a data vector. The lower layer or the visible units receive input data that are either binary or real. The layers are connected by a matrix of symmetrical weights. Each unit in every layer is connected to each unit in every neighboring layer. DBNs are trained using a greedy learning algorithm where one layer is trained at a time in an unsupervised manner. It is easier to train a shallow network than a deeper network. A multilayer DBN is divided into simpler RBMs models that are learned sequentially. The greedy algorithm allows each model in the sequence to receive a different representation of the data. This is an efficient layer-by-layer procedure for learning top-down generative weights that determine how the variable in one layer is dependent on the variables in the layer above. Each layer takes the output of the previous layer as input and produces an output which is a representation of the data with a simpler distribution. In DBNs, individual layers are trained in an unsupervised manner whereas the final fine-tuning is done by adding a

linear classifier to the top layer of the DBN and performing a supervised optimization.

5.4. Generative Adversarial Network

Generative Adversarial Networks (GANs) consist of two main components: a generative neural network and a discriminator neural network [65]. The generator network produces synthetic data in line with the properties of the original real dataset. The output from the generator is directly connected to the input of the discriminator. The discriminator network is fed data either from the training set or the data produced by the generator network, and it is tasked with predicting whether the data belongs to the training dataset or not. The classification performed by the discriminator provides a signal that the generator uses to update its weights through backpropagation. Training GANs is done as a competition between the generator and the discriminator. The discriminator network tries to maximize the difference between the real and the generated data, whereas the generator network tries to minimize the difference between the real and generated data.

6. Liver, lesion and vessel segmentation challenges

Several global competitions also known as segmentation challenges were organized by a few multidisciplinary organizations applying image processing techniques on medical images. In some of the earliest challenges such as SLiver07 [16] and LiTS 2008 [17], the participants applied traditional segmentation methods such as deformable models, statistical shape models followed by machine learning approaches including AdaBoost and SVM classifiers to liver and lesion segmentation tasks. However, DL-based methods were applied in LiTS 2017, the Combined Healthy Abdominal Organ Segmentation (CHAOS) and Medical Segmentation Decathlon (MSD) challenge. In this section, we first summarize the challenges dedicated to the DL-based liver, vessels and lesion segmentation. Next, we introduce a well-known publicly available dataset (3D-IRCADb) related to the liver, liver lesion, and vessel data along with ground truth.

6.1. LiTS 2017

LiTS [18] challenge was organized in conjunction with ISBI 2017 and MICCAI 2017. In ISBI 2017, the challenge was to segment lesions in the liver from CT images using automatic methods. In MICCAI 2017, in addition to lesion segmentation, liver segmentation and tumor burden estimation tasks were added. The dataset used in the challenge consisted of 170 contrast-enhanced abdominal CT scans, 130 were used for training and 40 for testing. Most of the methods proposed in ISBI 2017 and MICCAI 2017 were DL-based. Dice score was used as the main metric to evaluate the segmentation performance in addition to other metrics. Overall, the liver segmentation approaches achieved higher dice scores (around 0.90), whereas lesion segmentation approaches attained comparatively lower dice scores (0.70s).

6.2. CHAOS 2019

CHAOS challenge [66] was held in conjunction with ISBI 2019. The CHAOS challenge aims to provide the DL-based solution for five different tasks including segmentation of liver from CT, segmentation of the liver from MRI, Segmentation of liver from both CT and MRI, segmentation of abdominal organs from MRI and segmentation of abdominal organs from both CT and MRI. The CHAOS challenge dataset consists of abdominal CT and MRI images (T1-Dual and T2 SPIR sequences) from different patients. The CT dataset consists of 20 training set with the ground-truth mask for the liver and 20 testing sets. The MRI dataset consists of 20 training sets and 20 testing sets. The ground-truth mask for the liver, kidney and spleen is provided for the training dataset.

The task-specific conclusion of the CHAOS challenge revealed that the DL methods applied to liver segmentation performed as well as their semi-automatic counterparts on a single modality (both MRI and CT) when evaluated using the DICE score. However, the methods did not perform comparably for distance-based measures such as Maximum symmetric surface distance(MSSD). Furthermore, the performance of liver segmentation methods deteriorated in cross-modal approaches.

6.3. MSD dataset and challenge

MSD [67] dataset aims to provide an open-source comprehensive benchmark to solve different segmentation tasks for several organs. MSD challenge was held during MICCAI 2018. The MSD dataset consists of 10 labeled datasets including two dedicated to the liver, liver tumor, and liver vessel annotated data. Out of these, one dataset (liver and tumor annotations) consists of 201 contrast-enhanced CT images collected from various clinical sites in Europe and America. The patients included in this dataset had primary and metastatic liver cancers. The other dataset comprising 443 liver CT scans was acquired from Memorial Sloan Kettering Cancer Center. However, the annotations (vessels and tumors) are not very accurate. Statistics indicate that nearly 65.5 % of vessel pixels are unlabeled while about 8.5 % are mislabeled in this dataset Xu et al. [68].

6.4. 3D-IRCADb

3D Image Reconstruction for Comparison of Algorithm Database (3D-IRCADb) [69] is a well-known database administered by the French Institute of Digestive Cancer Treatment. It comprises various organs' data along with the corresponding segmentation of important structures. This database contains a relatively smaller quantity of liver data, that is only 20 abdominal CT scans with the liver and vessel annotation, however, the annotation quality is sufficiently high.

7. Evaluation metrics

In this section we describe a collection of relevant metrics used for evaluating the methods of the selected article. Some of the metrics discussed here could be derived from the four basic cardinalities of the confusion matrix namely true positive (TP), true negative (TN), false positive (FP) and false-negative (FN).

7.1. Accuracy (ACC)

Accuracy is the number of all correct predictions divided by the total number of samples in the dataset.

$$ACC = \frac{TP + TN}{TP + TN + FP + FN} = \frac{TP + TN}{P + N} \tag{1}$$

where P and N are real positive and negative cases respectively.

7.2. Sensitivity (SN)

Sensitivity is the number of true positive predictions divided by the total number of positives. It is also called as true positive rate (TPR) or recall (REC) and it is given by

$$SN = \frac{TP}{TP + FN} = \frac{TP}{P} \tag{2}$$

7.3. Specificity (SP)

Specificity is the number of correct negative predictions divided by the total number of real negatives. It is also called a true negative rate (TNR) and it is given by

$$SP = \frac{TN}{TN + FP} = \frac{TN}{N} \tag{3}$$

7.4. Precision (PREC)

Precision is the number of correct positive predictions divided by the total number of positive predictions. It is also called a positive predictive value (PPV) and it is given by

$$PREC = \frac{TP}{TP + FP} \tag{4}$$

7.5. Dice score (DICE)

DICE or F-measure is one of the most commonly used evaluation metrics in metrical image segmentation [70]. It is also called an overlapping index. In addition, to compare the segmentation result with ground truth data, DICE also measures reproducibility. The value of DICE lies in the interval [0, 1] where 1 is the perfect segmentation. A and B are the segmentation and ground truth respectively.

$$DICE(A, B) = \frac{2|A \cap B|}{|A| + |B|} \tag{5}$$

7.6. Jaccard similarity coefficient (Jaccard)

Jaccard coefficient also referred as Intersection over Union (IoU) is a similarity measure that estimates the common number of voxels between the segmentation result and the ground truth regions over their union.

$$Jaccard(A, B) = \frac{|A \cap B|}{|A \cup B|} \tag{6}$$

7.7. Volumetric overlap error (VOE)

VOE is the complement of Jaccard similarity coefficient.

$$VOE(A, B) = 1 - \frac{|A \cap B|}{|A \cup B|} \tag{7}$$

7.8. Relative volumetric difference (RVD)

RVD is a asymmetric metric and it is given by

$$RVD(A, B) = \frac{|B| - |A|}{|A|} \tag{8}$$

7.9. Average symmetric surface distance (ASD)

ASD is defined as the average of all the distances from the points on the boundary of segmentation to the boundary of ground truth and from the points on the boundary of ground truth to the boundary of segmentation, S(A) and S(B) respectively.

$$ASD(A, B) = \frac{1}{|S(A)| + |S(B)|} \left(\sum_{s_A \epsilon S(A)} d\left(s_A, S(B)\right) + \sum_{s_B \epsilon S(B)} d\left(s_B, S(A)\right) \right) \tag{9}$$

7.10. Root mean square symmetric surface distance (RMSD)

RMSD is commonly used as a statistical measure to show the magnitude of a varying quantity. The Smaller the RMSD value is the higher the similarity between the ground-truth and the segmentation is.

$$RMSD(A, B) = \sqrt{\frac{1}{|S(A)| + |S(B)|}} \times \sqrt{\sum_{s_A \epsilon S(A)} d^2(s_A, S(B)) + \sum_{s_B \epsilon S(B)} d^2(s_B, S(A))} \tag{10}$$

7.11. Hausdorff distance (HD)

HD provides a metric related to the degree to which two boundaries match. Hence it allows evaluating the adjustment of the boundary of the predicted segmentation and the ground truth. It is defined as shown in Eq. (12), which computes the maximum distance between the closest points of the two boundaries. However, because the lack of symmetry, the generalized form is used instead (see Eq. (11)) [71,72]. This is also known in the literature as the Maximum symmetric surface distance (MSSD).

$$HD(A, B) = max\{h(A, B), h(B, A)\} \tag{11}$$

where

$$h(A, B) = \max_{a \in A} \left(\min_{b \in B} d(a, b) \right) \tag{12}$$

In practice, the modified 95 % HD is used instead. This is the 95th percentile of the computed distances. Thus, limiting the sensibility of the HD to outliers [73,74].

7.12. Area under curve (AUC)

The ROC curve (Receiver Operating characteristic) is a plot that visualizes the tradeoff between the true positive rate and the false-positive rate of a classifier. In the case of *probability* classifiers, whose ROC curve has different points for different thresholds, the Area Under the ROC Curve (AUC) is a scalar used to summarize the performance of such classifier. It can be computed using the trapezoidal method to integrate the ROC curve [75].

8. Selected articles survey

This section reviews the selected collection of publications. For convenience, a summary table with the best performing solutions for each task i.e., classification, detection, and segmentation of liver, lesions or vessels, is included here (see Table 1). The complete list of articles can be found in Tables A.1 to A.5, in Appendix A. In these tables, the papers have been grouped based on the task: detection, classification, segmentation of the liver, segmentation of lesions or segmentation of vascular structures. However, for the analysis of the state of the art, the articles have been classified, based on the pipeline design (Fig. 9). Fig. 9 gives an overview of the pre-processing techniques, DL methodologies, patch processing and post-processing methods used in the papers reviewed. The vast majority of the published research operates on CT images and few works with MRI and ultrasound modalities. Most of the published works deal with the segmentation or classification of the liver parenchyma and/or lesions. Few groups work on segmenting the vessels like Huang et al. [139]; Ibragimov et al. [140]; Kitrungrotsakul et al. [82,141]; Lee et al. [165]; Yu et al. [147]; Mishra et al. [142], which we believe is of high relevance for surgical navigation.

8.1. Pre-processing

In the pre-processing step, the aim is to alter the nature of the image to highlight relevant features or adapt its intensity range to more manageable values for the model to process.

As aforementioned, the majority of the published research focuses on CT images. Hence, clipping the Hounsfield units (HU) to the relevant range for the anatomical structure to be segmented is common to these publications [77,91,92,110,121,125,127,129,130,132,134,166].

Table 1
Top ranking methods in the five analysed tasks: classification (C), detection (D), and segmentation (S) of liver parenchyma (Li), lesions (Le) and vessels (Ve) (Modal - modality, Dim - dimension, DSC - DICE score, ACC - Accuracy).

Author	Tasks	Method	Modality	Dim	Metrics	Dataset
Li et al. [76]	LiS	HM	CT, MR	2D	DSC(CT)-98.1, DSC(MR)-93.5	LiTS, CHAOS
Qin et al. [77]	LiS	CA	CT	2D	DSC-97.3	LiTS
Hu et al. [78]	LiS	HM	CT	3D	DSC-97.25	SLiver07, Clinical
Abdalla et al. [79]	LeS,LiS	HM	CT	2.5D	DSC-96.2	LiTS
Jiao et al. [80]	LeS	CM	CT	2.5D	DSC-96	TCGA-LIHC
Ouhmich et al. [81]	LeS, LiS	CM	CT	2D	DSC(Li)-89.9, DSC(Le)-90.5	Clinical
Kitrungrotsakul et al. [82]	VeS	EC	CT	2D	DSC-96	3DIRCAD, VascuSynth
Kazami et al. [83]	VeS	HM	CT	3D	DSC(HV)-90, DSC(PV)-94	Clinical
Kitrungrotsakul et al. [84]	VeS	EC	CT	3D	DSC-87.9	Clinical
Mostafiz et al. [85]	LeC	CA	US	2D	ACC-98.4	Clinical
Hassan et al. [86]	LeC	CA	US	2D	ACC-97.2	Clinical
Mitrea et al. [87]	LeC	EC	US	2D	ACC-97	Clinical
Fabijańska et al. [88]	LeD	CA	MR	2D	ACC-98.5	Clinical
Todoroki et al. [89]	LeD	CA	CT	2D	ACC-84	Clinical
Wojciechowska et al. [90]	LeD	CA	MR	2D	ACC-83	UK BioBank

However, the HU range is subject to the presence or not of contrast during the scan. The intensity clipped images can be further used to crop or extract patches from the regions of interest, e.g. Ahmad et al. [91,92].

Other techniques are commonly observed, e.g. isotropic resample [123], noise reduction [91,92,125], zero mean normalization [91–93,103] or min-max normalization [129,130].

Contrast enhancement techniques are mostly observed when working with MRI, e.g. in the work of Mulay et al. [104] where Contrast-Limited Adaptive Histogram Equalization is used to improve the contrast of abdominal MRI images. Though these techniques can also be found applied on CT images, like in Abdalla et al. [79]; Ahmad et al. [92] where histogram equalization is used.

During training, the data augmentation techniques like rotation, flipping, shifting, scaling were commonly used [81,120,125,126,129,133,139,147,155] to get more training data and prevent overfitting specific to the dataset. The other augmentation techniques were also observed, e.g. sharpening [104], adding Gaussian noise [81], changing the aspect ratio [156], elastic distortions [104,147], cutout augmentation techniques [93].

8.2. Methodology based categorization

The articles have been classified, based on the methodology of how the DL models are adapted into their developed frameworks (Fig. 9: *DL Methodology*). The main categories are:

1. Cascaded models: a two-steps pipeline where two models are connected sequentially. In this, the output of the first model is fed onto the second model. Both models use the same network architecture.
2. Hybrid models: a combination of different architectures, where each model is responsible for a different task.
3. Combined approach: a combination of DL approach and more traditional computer vision models for image analysis.
4. Ensemble classifier: three models with the same or diverse architecture are trained to analyze the slices along each of the anatomical axes or features independently. The result is then combined through a fully connected layer.
5. End-to-end learning / single-step approach: a single model is trained to perform series of tasks in one step.
6. Atlas-registration: a segmented anatomical atlas is used as a reference to segment the images by registering both together.
7. Detection guidance: an object detection model provides a heat map of the target regions to segment to the segmentation model.
8. Domain adaptation: the main goal here is to transfer knowledge from source (S) to target (T) to perform a specific task on T that is being shared by S and T [167].

The papers using multiple approaches/methodology are classified in the most relevant category.

8.2.1. Cascaded models

Christ et al. [125], Bi et al. [121], Vorontsov et al. [137], Kaluva et al. [130], Chlebus et al. [123] and Ouhmich et al. [81] are examples of cascaded networks, where the liver and lesions are segmented/detected in a sequential multi-step pipeline. In these cases, the method was tailored for CT images. A joint liver and lesion segmentation method based on the fully convolutional network (FCN) [168] model is proposed by Vorontsov et al. [137]. The network consists of two U-net like FCN models with long and short skip connections. The axial CT slices are given as the input to the first FCN which segments the liver region of interest (ROI). Unlike Christ et al. [125], for the second FCN, the axial slice along with the predicted liver ROI is given as the input and outputs the segmented lesions. In Christ et al. [125] the liver ROI segmented from the first FCN alone is given as the input to the second FCN. The method was further extended in Christ et al. [126] to segment liver and lesions from both CT and MR images. Segmented lesions from the MR images are further classified for malignancy and used for HCC survival prediction. Ouhmich et al. [81] proposed a cascaded FCN architecture based on Christ et al. [126] to segment liver parenchyma, liver lesions and necrosis hierarchically from 2D CT scans. Firstly, the method in which all structures are segmented simultaneously from the input is compared with the cascaded approach to segment structures hierarchically, and the cascaded approach performs better by reducing the false positives. Secondly, considering the cascaded architecture, the performance based on single-phase and multiphase CT scans are compared in which the multiphase approach has a better segmentation DICE score compared to the single-phase approach.

Kaluva et al. [130] proposed a two-step cascaded approach to segment the liver and tumors using densely connected FCN (DenseNet) [169]. In step 1, the liver model was trained to segment the liver. In step 2, the tumor model uses the first stage segmentation for the localization of the liver and hence performs tumor segmentation inside the liver region. In Chlebus et al. [123], the 2D U-net model is trained using axial, sagittal and coronal slices. To refine the liver mask, a 3D U-net is used. The liver segmentation has been achieved by classification of all voxels in the CT volume, tumor segmentation by classification of liver voxels and tumor candidate filtering using random forest (RF). Bi et al. [121] proposed a cascaded deep residual net (Cascaded ResNet) with multi-scale fusion to segment the liver and lesions from CT slices. ResNet [170] has skip connections between the convolution layers, which overcomes the training problem occurring in deep nets and makes it possible to add more layers to learn additional discriminative features. To further refine the segmentation output, Vorontsov et al. [137], Kaluva et al. [130] and Chlebus et al. [123] used connected component

analysis. In addition to the segmentation refinement, Christ et al. [125] used 3D conditional random field(CRF) to account for the 3D information.

Roth et al. [108] and Jiao et al. [80] proposed a two-step coarse to fine segmentation method. In Roth et al. [108], a multi-class FCN segments multiple organs including the liver from abdominal CT volumes. The search space of the first step FCN is reduced by using the mask of the body using simple thresholding to roughly delineate the structures. Then the prediction from the first step FCN is hierarchically fine-tuned by the second and it focuses more on the boundary regions. This method is based on the 3D U-net architecture by Çiçek et al. [171]. A 2.5D approach to segment liver tumors in CT images using a combination of two CNNs was proposed by Jiao et al. [80]. Three-phase images, i.e. arterial, portal vein phase and delayed phase are fed to the network as input. The input data is converted to CNN compliant values. True tags are created and stored as segmented tags for training. All the pixels in the training set are marked according to the true label. The first CNN outputs the probability value of tumor or non-tumor for each input. The second CNN thoroughly evaluates the pixels coming from the first CNN and assigns a class to each pixel. The method was evaluated using the cancer genome atlas liver hepatocellular carcinoma (TCGA-LIHC) dataset [172].

In Ben-Cohen et al. [120], the two visual geometry group (VGG) based FCN models were used where the first FCN segments the liver and the second FCN detects the lesions from the segmented liver. Three consecutive slices are given as input to provide spatial information in the three anatomical axes. Experiments conducted proved that the network learned the lesion texture and is most likely relying on the intensity difference between the liver and the lesions.

8.2.2. Hybrid models

Combining the features from different DL architectures, hybrid models were proposed for the segmentation [76,78,79,83,93,94,104,111,112,114,127,129,132,134,142,147] and classification [150,153,155] tasks. The U-net based models were proposed in Li et al. [132]; Han [127]; Yu et al. [147]; Wang et al. [111]; Li et al. [76]; Yan et al. [146]. Li et al. [132] proposed a hybrid densely connected U-net (H-DenseUNet) to segment liver and liver tumors from CT volumes. The simple ResNet architecture is used to get the coarse liver segmentation. The patches from the segmented liver are used as input to the hybrid net. The H-DenseUNet consists of a 2D Dense U-net that receives the advantages of both densely connected paths and U-net, which extracts the features from the intra-slices. Then, an auto-context algorithm hierarchically aggregates 3D volumetric information from the inter-slice correlations by integrating high-level visual features. In Han [127] the network architecture has two Deep CNN (DCNN) models that use long-range concatenation connections from U-net [173] and short-range residual connections from ResNet [170]. The proposed method segments the liver and lesions from CT. The model has 32 layers taking a stack of five consecutive CT slices as input, which provides significant information also in the axial depth direction in addition to the contextual information from the orthogonal slice. The models produce the output segmentation map corresponding to the center slice. The first model segments the liver from the input images whereas the second model segments the lesions from the segmented liver. To refine the segmentation, a 3D connected component labeling method is applied. Though the architecture performance is good for the liver, the performance on lesion segmentation is rather low Table A.2. Similar to Han [127], Yu et al. [147] proposed a 3D Residual U-net for portal and hepatic vein segmentation in CT scans. The residual block is incorporated into all convolution layers to propagate global and local information efficiently across the network. The residual module in ResNet is included in the 3D U-net for feature extraction in an effective way. Wang et al. [111] proposed a liver segmentation method using a 2D U-net and transfer learning approach. In the initial phase, the 2D U-net was trained with 300 unenhanced multi-echo spoiled recalled gradient echo (SPGR) MR images. The second phase consists of a transfer learning approach for generalizing the network to be applied for other imaging methods and tissue contrasts with 30 contrast-enhanced CT and MR images. The liver volume is computed from the segmentations and further used to estimate hepatic proton density fat fraction (PDFF).

Li et al. [76] proposed attention-based nested U-net (ANU-net) for abdominal segmentation where the nested U-net with encoder and decoder are arranged symmetrically on both sides of the network. For extracting more efficient hierarchical features, the context information extracted by the encoder is propagated along with the decoder through the dense skip connections. The model integrates an attention gate and deep supervision mechanism to focus on the target organ suppressing the irrelevant tissue. The dense skip connections of ANU-net obtain the feature maps at semantic levels. The proposed method was evaluated on both CT and MRI images. Similar to Li et al. [76], Dou et al. [94]; Yan et al. [146]; Mishra et al. [142] proposed deep FCN with the deep supervision for the robust segmentation of the liver and liver vessels respectively. In Dou et al. [94], supervision is applied in the 3rd and 6th layers of the FCN. The CRF is used as a post-processing step to improve the 3D liver segmentation. The 3D Deep Supervision Network (DSN) converges much faster than the regular 3D CNN and achieves fewer training or validation errors. It overcomes the vanishing gradient problem as well as improves optimization and enhances the discriminative capability of the model. This method has been further evaluated in Dou et al. [95] with many other experiments analyzing the underlying design principles and evaluated to segment the whole heart and the great vessels from the MICCAI 2007 HVSMR challenge volumes. With the objective of liver vessel segmentation, Yan et al. [146] proposed a novel liver vessel segmentation (LVSnet) architecture that employs special designs to accurately extract vessel structure. The attention-guided concatenation (AGC) module was developed to select useful context features from low-level features guided by high-level features. An innovative multi-scale fusion block has been introduced by constructing hierarchical residual-like connections within a single residual block. An automatic stratification method to split major and minor liver vessels was proposed to evaluate the effectiveness of this method in minor vessels. With base architecture as U-net, the attention-guided concatenation module was introduced between corresponding encoding and decoding layers. The multi-scale feature fusion block replaced the basic encoder and decoder blocks of the U-net. The study also presents a new dataset that consists of 40 different CT volumes for training and evaluation of liver vessel extraction algorithms. The proposed method in Mishra et al. [142] solves the problem of vessel segmentation from US images by decomposing it into two sub-problems. The first was the discrimination of object of interest from the background; coarse layers in the network in combination with auxiliary layers were trained to accomplish this task. Secondly, core layers with fine resolution were trained to learn the boundary of objects. The method was robust in retaining broken vessel boundaries, an issue frequently encountered in US image segmentation. The integration of the attention mechanism in the network enabled it to learn contextual information without enlarging the receptive field. Kazami et al. [83] presented a comparative study between the tracking-based (TA) algorithm and the supervised deep-learning-based algorithm (DLA) in extracting portal vein and hepatic vein from CT images. The multitasked 3D FCN method comprised vessel extraction, center voxel detection, and tree reconstruction. The method uses one encoder and three decoders for the above tasks. All the vessels from the image are extracted using a vessel decoder where the centerness decoder is allocated for extracting center-voxels in the vessel regions, and a topologic distance decoder is designed to learn the connectivity between center-voxels (topologic metric learning). The results from this study exhibit greater efficiency of DLA over TA algorithm in terms of sensitivity, specificity, and Dice coefficient.

Tian et al. [134] and Liang et al. [150] used the combination of a CNN and a long short-term memory (LSTM) for two different purposes. In Tian et al. [134] the authors proposed a novel multimodal data and

knowledge sharing framework between CT slices and textual reports with a semi-supervised attention mechanism. This method employed both a segmentation model and a language model, where the segmentation model is an FCN network for segmenting CT slices and a LSTM model is used as the language model for generating captions. In the FCN, segmentation predictions for the liver and tumor masks are done separately using two different branches. The segmentation masks generated by the FCN model will be passed on to a CNN to embed the visual features. The attention mechanism combines these features with the hidden state of the LSTM. In Liang et al. [150] the framework was proposed for the classification of focal lesions from multi-phase CT scans. This is an extension of Liang et al. [151] where they proposed a method using residual convolutional neural networks with global and local pathways (ResGLNet) to classify focal liver lesions only from a single-phase CT. In Liang et al. [150] the first ResGLNet part of the framework consists of three ResNet blocks that extract local and global information from the three respective CT phases. A random-walk-based segmentation algorithm is used to segment healthy and focal lesions. Patches are obtained from the segmented focal lesions corresponding to the four labels cyst, focal nodular hyperplasia (FNH), HCC and hemangioma (HEM). The second bi-direction LSTM (BD-LSTM) part consists of two LSTM layers that work in the opposite direction to extract enhancement patterns and anti-enhancement patterns from the sequential data. The ResGLNet and BD-LSTM are combined to employ multi-phase CT images as sequential data and to classify the focal lesions. The output of the three ResGLNet blocks serves as input to the BD-LSTM. The output from the BD-LSTM layers representing patches constitutes inputs to the fully connected layer. The softmax layer after the last fully connected layer gives the result of the patch-based classification.

Meng et al. [153] and Mulay et al. [104] developed hybrid models by incorporating VGG models into their framework. A method for liver Fibrosis classification in US images based on transfer learning and an FCN is proposed in Meng et al. [153]. The network has two stages. In the deep feature extraction stage, transfer learning using the VGG model trained on the ILSVRC dataset [174] is used to fine-tune the net for the 3-way liver fibrosis classification. The heat maps are the feature maps generated as output from the first stage. In the classification stage, the FCN is used to classify the feature maps into three classes normal liver, early-stage fibrosis and late-stage fibrosis. A method to segment the liver in 2D multimodal images was proposed by Mulay et al. [104]. This FCN based method combines holistically nested edge detection (HED) with mask-region-based convolutional neural networks (mask-RCNNs) [175]. The HED network is capable of capturing significant hierarchical representations from the multimodal data and is better able to discriminate organ contours. The HED network is initialized using VGG [176] model weights. The preprocessed images are input to the HED network that outputs refined edge maps; these maps are multiplied with enhanced images and input to mask-RCNN which finally segments the liver from the edge map images. A ResNet 101 FPN was used for feature extraction in mask-RCNN.

DenseNet based frameworks were developed in Chung et al. [93] and Abdalla et al. [79]. For liver segmentation and to address the volumetric image segmentation problem from CT scans, Chung et al. [93], proposed a method using a self-supervising scheme concerning the edge and contours. The authors utilized the properties of V-net [177], deep supervision mechanism and DenseNet. The proposed method applies two different deep supervision mechanisms for shape and contour. Depth-wise separable convolutions are introduced in densely connected blocks. The method implied that the use of critical and partial contour features instead of fully supervised contours could improve the segmentation process. Hu et al. [78] also incorporated the shape information into the CNN pipeline using a hybrid model. The segmented liver using CNN is thresholded and acts as a shape prior. To refine the initial segmentation a novel energy function that learns the multiple intensity distribution and appearances from the shape prior in the form of global and local statistics is proposed and globally optimized in a surface evolution way. In Abdalla et al. [79] the proposed hybrid network utilizes the features extracted from a 2D DenseUNet and 3D DenseUNet for segmenting liver and liver tumors from CT scans. The 2D dense network focuses on the slice features whereas the 3D dense network incorporates the spatial information. This enables the network to extract the inter-slice and intra-slice features.

Romero et al. [155] implemented a hybrid architecture by incorporating the Inception model within the CNN for classification. The method classified colorectal metastasis in liver CTs. The lesions are segmented using Vorontsov et al. [137]. All volumes are cropped to the size of the bounding box generated by the segmentation. The proposed method leverages the feature extraction capabilities from Inception V3 and Inception ResNet-V2. The patches from three adjacent orthogonal slices are used as input and the features extracted from multi-scale patches are concatenated at the end of the inception model. Two fully connected layers are used for classification. The method was evaluated using UK Biobank dataset [178].

The adversarial network is combined with a convolutional encoder-decoder in Yang et al. [114] and with DeepLab in Xia et al. [112] to segment the liver from CT data. In Yang et al. [114] a deep image-to-image network (DI2IN), a convolutional encoder-decoder model is trained with multi-level feature concatenation and deep supervision end to end. Then the GAN is used as a discriminator to differentiate the output generated from a DI2IN and the ground truth. The adversarial network is no longer required during inference after the training process. The network uses both the local and global contextual information to train the model and proved to be better than U-net and DSN for 3D segmentation with substantially faster processing speeds. Pix2pix is used as GAN in Xia et al. [112]. Deep features and semantic features are used to realize the segmentation model. The proposed segmentation framework comprises three components: the semantic segmentation model realized using DeepLabv3, the generator to reconstruct the image from training data and the discriminator to identify the real and reconstructed image. The generator is built as a codec network. Skip connections are added among the layers to cascade features of one layer with the other. This combination not only yields better segmentation outcomes; moreover, it shows stability in terms of convergence while training. Jiang et al. [129] designed an Attention Hybrid Connection Network architecture (AHCNet) which combines soft and hard attention mechanisms with long and short skip connections. A AHCBlock consists of the attention gate (AG) module and the hybrid connection module. The AG module performs feature selection on the coarse-scale context information obtained by the long skip connections to improve the sensitivity of the model to the foreground pixels. AHCNet integrates the higher-level semantic features and the lower-level location information by combining both long and short skip connections and soft attention mechanisms to complete the fine-grained in-formation recovery of the medical image. It is a cascaded approach based on the liver localization network, liver segmentation network, and tumor segmentation network. Xu et al. [113], proposed a different strategy using a growing teacher assistant network (GTAN). It is a DL-based real-time 3-D liver CT segmentation method using the knowledge distillation (KD) also known as knowledge transfer from teacher to student models. It is incorporated to compress the model while preserving the performance. To avoid the KD training being stuck at the local minimum when the disparity of teacher and student model sizes is large, the self-distillation modules were incorporated. The proposed method was compared to the student model without KD and shows a significant improvement of 1.2 % in the Dice coefficient. The inference time reported for the GTAN model is 13 ms per a 3D image and is proposed to have a great potential for intervention in liver surgery as well as in many real-time applications.

8.2.3. *Combined approach*

Traditional computer vision algorithms including Markov Random Fields (MRF), graph-cuts, deformable models, active contour were either used for initial segmentation ([77,86,88,89,159]) or used in the final

step for segmentation refinement [92,98–101,103,138,140,143]. Supervised models like SVM have also been used for classification [85] in the combined pipeline. In Wu et al. [159], the sparse non-negative matrix factorization method is used to extract the Time Intensity Curve (TIC) from the pre-processed CEUS videos. Then, a DBN is used to classify benign and malignant focal lesions on these TICs. Ibragimov et al. [140] proposed a 3D CNN for the automatic segmentation of the portal vein (PV) from the CT images. The intensity patterns of the PV are quite distinguishable from other structures in the image, where the trained CNN extracts these patterns and uses them to enhance the vein in the target image. Using MRF the enhancement results from the CNN will be additionally smoothed for more precise enhancement. Finally, the CNN-MRF-based enhancement method is expanded with PV centerline detection based on the PV anatomical properties such as tubularity and branch composition. Mitta et al. [103] method aims to tackle the problem of relying on manual segmentations by addressing the problem using an unsupervised learning approach. The authors used modified W-net [179] architecture and introduced attention gates to the skip connections to suppress the noise in segmentation. The network was modified to be applied on 3D volumes and utilizes conditional random fields for post-processing.

Lu et al. [100]; Guo et al. [98]; Ahmad et al. [92] used active contour models to refine the initial segmentation from the DL models. Lu et al. [100] trained a CNN model to get the coarse segmentation of the liver volume. The active contour method was further used to refine the segmented liver. In Guo et al. [98], the label map is created such that the image carries manifold information such as if a pixel exists inside or outside the object of interest if it is located on the boundary of the object, and how distant it is from the border. Inspired by the FCN-8 architecture, the proposed network uses an FCN and learns manifold category information corresponding to only one possible object class that is liver. The network output then guides the active contour model to regulate the evolution of the contour. The proposed architecture combines information from the FCN and active contour models which is capable of steering the expansion of the contour and better conserves the geometry of the liver. Ahmad et al. [92] proposed a DBN-based method to automatically segment the liver. The method is based on training a DBN for automatic feature learning by unsupervised pretraining and supervised fine-tuning named DBN-DNN collectively. After completing the unsupervised training layer by layer, the network is fine-tuned concurrently in all layers. Finally, a 3D active contour method is used for liver segmentation refinement.

Qin et al. [77] proposed a superpixel-based and boundary-sensitive CNN pipeline for the automatic segmentation of the liver. At first, CT images are partitioned into superpixel regions. In this method, the conventional binary segmentation problem is converted into a multinomial classification problem where the superpixels are labeled into the three classes; interior liver, liver boundary and non-liver background. The entropy-based saliency map is computed and leveraged to guide the sampling of image patches over the superpixels. This helps to explicitly identify the liver boundary. Finally, the CNN is trained to segment the liver. In Hassan et al. [86], a combined classification and segmentation approach is proposed to diagnose focal liver diseases using a combination of level sets, fuzzy-C-means and autoencoders. The level set method and fuzzy-C-means clustering are used to extract the contour and segment the lesions from the preprocessed images. The stacked sparse autoencoders (SSAE) are applied to extract high-level features from the segmented ROI in an unsupervised manner from the unlabeled dataset. Finally, the softmax classifier is used to classify the ROIs into different focal diseases. Similarly, Mishra et al. [143] proposed classification and segmentation workflow to segment vessels. The images were first divided into overlapping patches. A simple CNN then classified each patch into a positive vessel patch if it completely or partly covers the region of a vessel or a negative patch if it does not contain the vessel at all. Three methods were applied to do pixel-level segmentation later including thresholding, region growing, and k-means unsupervised clustering. Out of these methods, k-means clustering gave the best results.

Irving et al. [99], Zheng et al. [138] employed FCN based models to segment the liver. In Irving et al. [99], the U-net like FCN is used followed by the simple thresholding method to get the final segmentation. In Zheng et al. [138], in addition to the liver, the tumors in the liver are also segmented along. The trained FCN is used to segment the liver and tumor regions coarsely, thereafter the segmented tumor is refined by the 3D deformable model. The deformable model is derived from a combined NMF and local cumulative spectral histograms. Compared to the other approaches, Masoumi et al. [101] proposed a combined approach using MLP and the watershed algorithm. The traditional watershed algorithm often causes over-segmentation in medical images. To overcome this problem, the MLP is trained to extract features of the liver region. These extracted features are used to monitor the quality of the segmentation performed by the watershed algorithm.

In Mostafiz et al. [85] the combination of a CNN and a SVM were used for the classification of fatty liver lesions. Deep CNN features were combined with local binary pattern and Gabor wavelet features in Mostafiz et al. [85] to extract features from liver ROI. A pre-trained VGG19 was fine-tuned and used for this purpose. Feature optimization was done to select the most relevant features and discard the irrelevant features. Besides, the Bayes rule selected the most informative image patches to improve processing time. The optimized feature set was then fed to a SVM classifier that classified the samples into two types: normal liver and liver lesions.

Todoroki et al. [89]; Fabijańska et al. [88]; Wojciechowska et al. [90] proposed methods to detect lesions from the segmented liver. In Todoroki et al. [89], the combined random walk and computation anatomy models were used to segment the liver. The liver lesions that belong to multiple classes like Cyst, FNH, cholangio cellular carcinoma (CCC), HCC and metastasis (Meta) were detected using the DCNN model. Fabijańska et al. [88] employed the combination of statistical shape models, thresholding and using active contours to segment the liver and the U-net based model to detect the lesions. The DCE-MRI volumes processed by averaging all three phases (before contrast injection, arterial phase, late phase) to a grayscale image is used as an input. Wojciechowska et al. [90] is distinct from Todoroki et al. [89]; Fabijańska et al. [88] by using a DL centered solution to segment the liver and traditional approaches to detect the lesions. In Wojciechowska et al. [90], the liver parenchyma excluding vessels is segmented using CNNs. Morphological operations are used to close holes such that the parenchyma includes the vessels and the cysts. The method employed intensity thresholding and circularity measures to detect the cysts inside the segmented liver region and differentiate the cysts from the blood vessels, bile ducts and other artifacts.

The methods from Qin et al. [77], Lu et al. [100], Zheng et al. [138], Ahmad et al. [92], Guo et al. [98], Todoroki et al. [89] were evaluated on CT, the methods from Irving et al. [99], Mitta et al. [103], Masoumi et al. [101], Fabijańska et al. [88], Wojciechowska et al. [90] were evaluated on MRI and Wu et al. [159], Hassan et al. [86], Mishra et al. [143], Mostafiz et al. [85] on ultrasound images .

8.2.4. Ensemble classifier

Kitrungrotsakul et al. [141], Kitrungrotsakul et al. [84], Kitrungrotsakul et al. [82] proposed a 2D multi-pathway network for vessel segmentation where the method is trained for binary classification based on patches extracted from three planes: sagittal, coronal and axial. Three separate CNNs are used to extract features from each of the planes and then the features from all the three CNNs are concatenated using a fully connected layer. The trained DNN classifies each voxel into vessel or non-vessel. The final segmentation image is gathered from the classified pixels/voxels. Kitrungrotsakul et al. [84] and Kitrungrotsakul et al. [82] were evaluated on clinical CT data. In Kitrungrotsakul et al. [141], the raw CT images were used as the input but Kitrungrotsakul et al. [84] and Kitrungrotsakul et al. [82] use a vesselness probability map as input

rather than raw CT image, which makes it robust and insensitive to the intensity changes. Using vesselness probability as the input seems to improve the segmentation results. In Kitrungrotsakul et al. [82], the method was validated extensively with more experiments on multiple datasets including 3DIRCAD and VascuSynth [180,181].

Wang [37] and Chlebus et al. [124] proposed a similar method using a tri-planar FCN based network for the segmentation of the liver and liver tumors. The architectures consist of three FCNs in which the patches from slices of sagittal, coronal and axial planes from the image volume are fed as input. In Wang [37], the liver is segmented initially and the resultant liver regions from all three planes are given as input to the three different FCNs which outputs the liver lesions. In Chlebus et al. [124], both the liver and tumor regions are segmented simultaneously by the U-net like FCNs followed by the thresholding and largest connected component analysis for the liver. In addition, the model uses different resolutions to accumulate the local and global features and employs skip connections. In both Wang [37] and Chlebus et al. [124], the outputs from the three FCNs are combined in the final step. Using the tri-planar approach shows a better segmentation performance for both the liver and the tumor in terms of DICE [124] and VOE [166]. The methods from Wang [37] and Chlebus et al. [124] were evaluated on the 3DIRCAD CT dataset, and clinical MRI dataset respectively.

Sun et al. [133] and Bi et al. [122] proposed a multi-channel FCN (MC-FCN) network for the purpose of segmentation. The network proposed by Sun et al. [133] is based on AlexNet [182] and has three input channels that can be used to extract features from three CE-CT images with independent parameters. The output feature maps from the three FCN channels are given to a softmax classifier to obtain the final prediction score. The method proposed in Bi et al. [122] works by embedding an FCN in a stacked architecture (stacked FCN architecture with multi-channel learning (SFCN-ML)) for learning the foreground ROI features and background non-ROI features separately and then integrating these different channels to produce the final segmentation result. The proposed method is said to apply to different types of ROIs including lesions and anatomical structures, various ROI locations, grayscale and color images, ROIs with varying contrasts/textures and regular as well as irregular shapes/boundaries. Mitrea et al. [87] combined B-mode US and CEUS to classify HCC lesions. The experiments were done using multiple DL architectures or classifiers to analyze the impact of combining both images directly or performing fusion at the feature level, classification level or decision level. Best results were obtained when both modalities were combined compared to individual modalities. Moreover, the arithmetic mean of the probability values from the classifiers used at the decision level combination was found to be the best performing. The effects of preprocessing and enhancement were studied for the task of hepatic vessel segmentation in Survarachakan et al. [144]. The combination of conventional preprocessing techniques, hessian-based vesselness filters (Frangi, Hessian, Sato, Meijering) and gamma filtering techniques were studied. The 3D U-net model was trained on each vesselness filtered image separately and the outcome is ensembled. Fusing the outcome improved the segmentation results significantly.

Meine et al. [102] investigated the performance of several 2D and 3D U-net based architectures for liver segmentation in CT images. It is possible to train and apply each of the FCN architectures mentioned in this paper on many voxels at once by feeding larger patches into the networks. The aforementioned methods were evaluated on a liver CT dataset and showed that an ensemble classifier of three 2D U-nets trained on orthogonal slices performed better than single 2D or 3D U-nets.

8.2.5. End-to-end learning approach

Li et al. [131], Frid-Adar et al. [163], Huang et al. [139], Tang et al. [110], Yu et al. [147], Schmauch et al. [156], Prasad et al. [107], Pandey et al. [105], and Gibson et al. [97] proposed Deep CNNs and Ahmad et al. [91] proposed deep-stacked auto-encoder (DSAE) for the purpose of segmentation. Li et al. [131] is a patch-based method in which patches containing lesions and normal tissues were used as positive and negative samples to train the seven-layer DCNN. The model segments liver tumors in CT images. Frid-Adar et al. [163] differs from Li et al. [131] by acquiring the patches of non-lesions extracted from the normal boundary and normal-interior as two classes. The probabilities from normal-boundary and normal-inside patches are combined and the final classification is lesion and non-lesion using a softmax classifier. This modeling seems to be more effective for learning from the patches. The images with different scales are used to obtain both the local fine details and global spatial information.

The methods proposed in Prasad et al. [107]; Huang et al. [139]; Thomson et al. [145]; Pandey et al. [105] are based on U-net models. Prasad et al. [107] proposed a modified version of U-net architecture for liver parenchyma segmentation in CT images. The primary objective of the proposed work seems to be to develop a network trained with a limited amount of data. The network is trained using a 3Dircadb dataset avoiding overfitting by following certain strategies such as adding Gaussian noise and early stopping criteria. Huang et al. [139] proposed an automatic method for robust liver vessel extraction from CT images using a dense 3D U-net architecture and a variant of the dice coefficient cost function. The method uses a dense 3D U-net architecture and data augmentation for training with few samples and incomplete annotations. 3D U-net was applied to vessel segmentation in the liver US and 2D stacked US images in Thomson et al. [145]. The number of filters in the original U-net was reduced in their approach due to computational load. The method performed worse than 2D segmentation methods [143], particularly in segmenting small bifurcations and branches near the edge of the volume. Furthermore, the model was trained on a small dataset. Pandey et al. [105] proposed a semi-supervised contrastive learning (CL) [183] framework based on the attention U-net for 2D segmentation tasks. The model is trained for the semantic segmentation task and the class-wise patches are obtained via pseudo-labels (the pixels belonging to the prominent class are retained in each sampled patch and the rest of the pixels are masked). The framework is trained on pseudo-labels of patch-wise embeddings. For better feature clustering, consistency regularization combined with CL is proposed.

A study aimed at developing liver segmentation techniques for CT of selective internal radiation therapy (SIRT) patients was presented in Tang et al. [110]. The proposed network is a modification of the 3D CNN which processes data in a multi-resolution fashion. Tang et al. [110] has an additional pathway that makes the CNN learn contextual information from the abdomen. In Gibson et al. [97], the liver is automatically segmented from laparoscopic videos using deep fully convolutional residual networks with multi-resolution loss functions. A combination of unsupervised feature learning and fine-tuning was applied in Ahmad et al. [91]. The features from the images are learned using DSAE in an unsupervised learning approach and fine-tuned using a softmax layer. Patch-based learning was adopted instead of pixel-by-pixel mapping which contributed to the reduction in the complexity of the training algorithm.

CNN based methods were proposed to classify liver lesions from CT [148,160], MR [158,161], and ultrasound [152,154,156] images. Ben-Cohen et al. [148] proposed a pixel-wise classification of CT images that included both benign and malignant hepatic lesions. The proposed model is U-net based which accepts a CT image as the input and outputs a per-pixel six class segmentation (background, interior liver, liver boundary, metastasis, hemangioma and cyst). Zhang et al. [161] proposed a method for the classification of the liver tissue types on 3D MR images consisting of one T2 weighted MR image and three T1 weighted dynamic contrast-enhanced images. The method classifies the liver parenchyma and the tissue that consists of viable tumors and necrosis. A novel CNN was introduced to capture the contextual information and perform classification of the local patch region. The method adopted a U-net architecture where the model takes the input patches sampled at different resolutions and predicts the output. The use of multi-resolution

input, auto context design and multi-phase training procedures improved the overall performance when compared with traditional U-net architecture. Trivizakis et al. [158] proposed a 3D CNN-based architecture for the classification of liver tumors as primary or metastatic from DW-MRI volumes. The proposed 3D CNN shows a better performance compared to 2D patch and slice-based methods. Yasaka et al. [160] investigated the diagnostic performance of CNNs for the differentiation of liver masses on dynamic contrast-enhanced CT. The research included the following five categories of liver masses; classic HCCs; malignant liver tumors; indeterminate masses; liver hemangiomas and cysts. During training, five different models were obtained for un-enhanced, arterial, delayed phase, triphasic, combined arterial/delayed CT images. The model trained on triphasic images showed better performance followed by combined arterial/delayed compared to the single-phase images. In Marya et al. [152], the ResNet50V2 initialized with ImageNet weights was used for extracting features from ultrasound images to classify malignant and benign lesions. A 3D-CNN was proposed Pan et al. [154] to identify FNH and HCC using temporal features in US videos. By incorporating temporal information with spatial features, the receptive field of the proposed CNN could be enlarged which results in higher classification accuracy. Sîrbu et al. [157] applied DCNN to classify FLL into five categories [3]: three malignant including HCC, Hypervascular Metastases (HYPERM), Hypovascular metastases (HYPOM) and two benign including Hemangioma and FNH. The authors performed empirical experiments to come up with optimal DCNN architecture by analyzing architecture complexity, hyper-parameters and optimization methods. This work was extended to diagnose FLLs using DNN and a hard voting scheme in Căleanu et al. [149]. A novel evaluation strategy leave-one-patient out (LOPO) was proposed in this work. Schmauch et al. [156] proposed a CNN-based approach to detect liver lesions, determine the malignancy and characterize the lesion type. The model is trained for all three tasks at the same time. ResNet50 is used for feature extraction; The images are fed to ResNet50 that output features which are further fed to the "attention block"; this block learns to identify abnormalities in images. The same features are fed to another part of the network which takes an average of feature maps on the designated regions. Finally, the densely connected layer predicts to which of the seven categories the detected lesions belong. The categories include malignancy, metastasis, carcinoma, cyst, and a few others. The method was evaluated on Journees Francophones de Radiologie 2018 (JFR18) dataset [184].

8.2.6. Atlas registration

Vivanti et al. [135] and Vivanti et al. [136] proposed a new approach for liver tumor segmentation in follow-up CT studies, which is quite essential in liver tumor therapy. As an initial step, the follow-up scans are non-rigidly registered to the baseline scans and the tumors were delineated from the follow-up scans after the registration. This is followed by using a CNN as a voxel classifier, which classifies and segments the known liver tumor voxels in the follow-up scans. The morphological operations are used to post-process the segmentation. In addition to tumor segmentation, Vivanti et al. [136] addresses tumor burden quantification. The registration of baseline and follow-up scans detect changes and regions of new candidate tumors in the follow-up scans. The candidate tumors are detected and segmented using a Chan-Vese level set method. Finally, the RF method is used for the classification of new candidate tumors. This method advances the method presented by Vivanti et al. [135] in which, only known tumors are segmented from the follow-up CT scans and new tumors are not detected.

FCN-based 2.5D approach was proposed in Jansen et al. [164] to segment the liver in six-phase Dynamic Contrast-Enhanced (DCE)-MRI images. Both DCE-MRI and DW-MRI images from the same patient were used to detect liver metastases inside the segmented liver. DW-MRI and DCE-MRI data are registered for motion correction. The proposed segmentation part of the network consisted of a dilated FCN model and 3D hole filling was applied on the resultant probability maps. For metastases detection, a two-path FCN was proposed; one path to accepting DCE-MR images and the second to feed DW-MRI images. Morphological closing and then opening were used for post-processing. Lee et al. [165] proposed an HCC lesion detection network for CECT images. As a first step, the liver is segmented from portal venous phase images using FCN-VGG16. For the learning 12 bit images are converted into 24-bit RGB images. Secondly, the segmented liver ROI is registered to all four phases using initial rigid registration and B-spline based non-rigid registration. For transfer learning, the registered 12-bit greyscale 3D volume images are converted to 24-bit 2D RGB images. The artery, portal venous, and delay phases are converted to 8-bit greyscale images and filled into the R, G, and B channels, respectively, resulting in a 24-bit RGB image for multi-phase learning. This is used as an input to DetectNet which is a modification of Inception v1 for HCC detection where the classification and detection are performed at the same time in parallel. As a postprocessing step, a 3D connected component method is used. Bousabarah et al. [162] developed a method based on DCNN for the liver and HCC segmentation. The main objective of this method was to automate the application of Liver Imaging Reporting and Data System (LI-RADS), where it is used for HCC diagnosis. The image sequence of venous and delayed phase images are registered onto arterial phase using similarity transforms with B-spline interpolation, and then used to train the model. The results from the DCNN are further processed using cluster thresholding and RF classifier to reduce false positives.

8.2.7. Detection guidance

Hoogi et al. [128], Tang et al. [109], Bellver et al. [119] proposed detection based segmentation approaches based on various CNN architectures and the methods were evaluated on CT images. In all three methods, the position of the liver is accurately marked with 2D bounding boxes which are further given to the segmentation model as input. The method proposed in Hoogi et al. [128] includes marginal space learning trained by Adaboost to detect the organs (liver, lymph nodes) and lesions. Then, the combined segmentation model incorporating generalized CNNs and active contour methods is applied to segment the lesions. It is also effective in handling lesions with low contrast and substantial heterogeneity within other organs. The method has a limitation when the lesions are heterogeneous. Tang et al. [109] proposed a detection and segmentation laboratory (DSL), where the detection is performed by the Faster R-CNN model, which produces a bounding box of the liver, and the DeepLab uses the pixels inside the bounding box to segment the liver. Bellver et al. [119] implemented an approach based on the Deep Retinal Image Understanding (DRIU) framework, a VGG-16 based network. The aforementioned framework has proven to be successful in the segmentation of the blood vessels and optical disk in eye fundus images. Once the predicted 3D bounding box was placed around the liver, the different slices cropped by this bounding box were segmented by the lesion segmentation network. For the post-processing stage, a 3D-CRF is added which models the conditional distribution of the output prediction.

8.2.8. Domain adaptation

In single-modality or cross-modality domain adaption (DA), it is assumed that the tasks and domain feature space remain the same whereas, source and target marginal distributions are different. The probability of rising in test error may occur in proportion with distribution difference between the source and target domain, often called the "domain shift" problem. DA is considered as a possible solution for addressing the domain shift or heterogeneity among medical images, thereby reducing the distribution differences between different but related domains. For cross-modality liver segmentation using DA, Yang et al. [115] proposed DA via Disentangled Representations (DADR). A shared domain-invariant content space and domain-specific style space are used here, where the images from each domain are embedded and DA performed in domain-invariant space. For multi-domain liver segmentation, You et al. [117] introduced a novel unsupervised DA method

where the authors used Wasserstein distance to obtain domain invariant representations. The method involves incorporating 3D volumetric information and a content discriminator that distinguishes extracted content-level representations between different domains. For enforcing many-to-many mappings, the method uses a cross-cycle consistency loss. An example of Domain Agnostic Learning (DAL) where the objective is to learn from a source domain and map to arbitrary target domains, Yang et al. [116]proposed Domain-Agnostic Learning framework with Anatomy-Consistent Embedding (DALACE). The objective is to learn a disentangled representation that is invariant of different imaging modalities but also preserving anatomical structures. This method achieved an average dice of 0.847 for the DA task and 0.794 for the DAL task. Utilizing the efficiency of DA in a broader spectrum, Fu et al. [96] proposed a method on Domain Adaptive Relational Reasoning (DARR), where the objective was to perform 3D abdominal multi-organ segmentation in datasets collected from different scanners and protocols. To obtain the spatial relationship, a puzzle module has been combined with the segmentation task for recovering CT images from shuffled patches. Pham et al. [106] uses zero-shot DA, where the segmentation model has been trained solely on the source domain and uses prior knowledge on both CT and MR for obtaining general features. A vanilla U-net with fixed Sobel kernels that enhances contour information and a convolutional autoencoder that learns anatomical priors were applied for the implementation. The method was extensively evaluated on CHAOS, TCIA [185], and Synapse[1] datasets. Zhou et al. [118] proposed anatomy-guided DA network for segmentation (APA2Seg-Net), without target modality ground truths. The method utilizes conventional CT images for training the robust CT CBCT/MR segmenters (segmentation model). A robust point matching (RPM) method to estimate the multi-modal registration information where RPM is guided by the anatomic information extracted by the CBCT/MR segmenters. APA2Seg-Net is a cyclic adversarial two-stage network, one with anatomy preserving DA network and a segmentation network. There exist five networks including two generators, two discriminators and one segmenter where one of the generators adapts images from CT to CBCT/MR domain, and the other adapts inversely whereas the discriminator identifies between real CBCT or adapted ones.

8.3. Patch processing

In the vast majority of the papers reviewed, DL models are trained on whole 2D slices or 3D patches for various tasks. Patch-based learning was adopted in Ben-Cohen et al. [120]; Qin et al. [77]; Frid-Adar et al. [163]; Kitrungrotsakul et al. [84]; Chlebus et al. [124]; Meine et al. [102]; Kitrungrotsakul et al. [82]; Li et al. [131]; Zhang et al. [161]; Romero et al. [155]; Trivizakis et al. [158]; Ahmad et al. [91,92]; Fu et al. [96]; Li et al. [132]; Liang et al. [150] to reduce the complexity of the training algorithm by using small patches instead of the entire volume. The pixels inside the non-lesions and their boundaries are heterogeneous so Frid-Adar et al. [163] extracted the patches of non-lesions from the boundary and their interior as two different classes.

In Bellver et al. [119]; Han [127]; Ben-Cohen et al. [120] the models were trained on three or five consecutive slices providing significant information in the axial depth direction in addition to the contextual information from the orthogonal in-plane direction. The models produce the output segmentation map corresponding to the center slice by incorporating spatial information from the neighboring slices. In Christ et al. [125]; Dou et al. [94]; Bellver et al. [119]; Ouhmich et al. [81], though the DL models were trained on 2D slices or patches, 3D post-processing techniques like CRF are used to obtain the depth information. Both the methods using consecutive slices or 3D post-processing on 2D methods are referred to as 2.5D methods. Compared to 3D methods, the computational complexity in 2.5D methods is less despite obtaining some depth information. Different from the aforementioned methods, [159] extracted Time Intensity Curves from the 2D frames of CEUS videos and used it as input to the model to distinguish tumor vs liver parenchyma.

8.4. Loss function

To tackle class imbalance in the dataset and to optimize the training model accuracy, different loss functions were proposed. In Çiçek et al. [171]; Jiao et al. [80]; Qin et al. [77]; Trivizakis et al. [158]; Jansen et al. [164], cross-entropy(CE) loss or its variant were used. The weighted voxel-wise CE loss [171], improved class equilibrium CE loss [80], sparse cross-entropy CE loss [158] were shown to perform better than the regular CE loss functions. Variants of Dice loss were used in Chlebus et al. [124]; Huang et al. [139]; Yu et al. [147]; Huang et al. [139]. Soft Dice loss [124] and weighted Dice loss [147] were shown to be better than normal Dice loss, particularly in terms of segmenting smaller structures. The joint loss functions combining multiple loss functions were proposed in Kaluva et al. [130]; Liang et al. [150]; Jiang et al. [129]; Xia et al. [112]; Zhou et al. [118]; Mitta et al. [103]; Li et al. [76]. In Kaluva et al. [130] the combination of the spatially weighted cross-entropy loss function and the DICE overlap coefficient is used. A new joint loss function that combines both the inter-loss and intra-loss between the classes is proposed in Liang et al. [150]. In Jiang et al. [129], the joint dice loss function is proposed to train the liver localization network and focal binary cross-entropy is used to fine-tune the tumor segmentation network. In Xia et al. [112] segmentation-based loss, content-based loss and adversarial loss are combined into a single loss function of Wasserstein GAN to assess the results. In [118], the combination of adversarial loss, cycle consistency loss, segmentation loss, identity loss and anatomy preserving loss together with Modality Independent Neighborhood Descriptor loss and correlation coefficient loss was used. The joint loss function using N-cuts loss and Reconstruction loss was used in [103]. The N-cuts and the reconstruction loss were used to optimize the encoder and decoder models respectively. Li et al. [76] uses a hybrid loss function combining soft Dice coefficient loss, focal loss and pixel-wise cross-entropy loss. Gibson et al. [97] proposed multi-resolution loss functions. Other loss functions such as the negative-log likelihood [82,84,94,131], non-normalized softmax [98] and SensSpec [99] loss functions were observed.

8.5. Post-processing

In the segmentation task, post-processing methods are used to refine the segmentation obtained from the DL model. The connected component analysis [123,127,129,130,147,165] and the morphological operators [79,91,121,130,135,164] are the most used post-processing methods followed by 3D CRF [81,94,103,119,125]. Kaluva et al. [130] utilized both the connected component analysis and morphological operations to further improve the segmentation results. 3D CRF is also used in some methods [125,126] to account for 3D information involving 2D DL models to get the initial segmentation. In the methods involving the combined approach, the traditional segmentation methods like active contour models [92,98], deformable models [138] and graph-cut methods [100] were used to refine the segmentations obtained from the DL models. The papers show that the post-processing methods improve the segmentation performance obtained from the DL models.

9. Discussion

Automatic precise detection, classification and delineation of the liver, lesions and relevant anatomical structures like major vessels is critical for computer-assisted diagnosis and treatment planning. Due to the availability of powerful computing machines, advancement in algorithms and digitization of medical images, DL methods have become widely used for medical image analysis. In the last decade, nearly 90

[1] https://www.synapse.org/#!Synapse:syn3193805/wiki/217752.

papers were published exclusively in DL-based liver image analysis. The intention to use DL-based methods is not just a trend, but also due to its high competence. The DL-based methods outperformed other traditional and machine learning approaches for liver segmentation ([94,95]; [77,81]) and lesion classification tasks [86,91,153,159].

9.1. Best performing methods

The 91 papers reviewed in this article (Tables A.1 to A.5) have been thoroughly analysed. The publications were categorized based on the methodology used (see Section 8.2). Even though the disparity in testing datasets e.g., public and private, and metrics reporting, we rank the performance of the proposed solutions based on the following criteria:

- segmentation performance is measured in terms of the Dice score,
- whereas classification and detection solutions are ranked based on the accuracy.

Both Dice score and accuracy are the most commonly used metrics, in each respective task.

In the tasks of liver segmentation, the three top methods based on Dice score were the following: Li et al. [76], Qin et al. [77], and Hu et al. [78]. Though DL-based methods have been proven to better perform compared to non-DL methods, the way data is handled, processed and fed to the network plays a crucial role. To the writers' knowledge, the liver segmentation method presented by Li et al. [76] achieved better results because of the multi-scale feature extractor strategy. Hence, simultaneously providing global and local context to the network. The same hybrid model strategy is followed by Hu et al. [78], which ranked third. However, unlike Li et al. [76], the latter did not use deep supervision and attention to extract the relevant features at the different scales. Instead, the network was trained to find the most relevant features. The method presented by Qin et al. [77], ranking second, aimed for a combined approach. However similar to the two aforementioned solutions in the sense that Qin et al. [77] also used a smart preprocessing of the images to use the most relevant features. Here superpixel patches were initially classified into *interior of the liver*, *liver boundary* or *outside of the liver*, using multimodal classification. Based on information entropy content, the three categories were sampled to build the training batches with patches containing relevant information. The final output was a probability map of the parenchyma boundary.

For lesion segmentation, the three best performing solutions were those presented by Abdalla et al. [79], Ouhmich et al. [81] and Li et al. [131]. Abdalla et al. [79] used a hybrid network by incorporating both the inter-slice and intra-slice features, resulting in better lesion segmentation. Whereas solutions by Jiao et al. [80] and Ouhmich et al. [81] share the use of cascaded methods, where two consecutive CNNs are used to segment both the liver and the tumors in CT volumes.

For the vessel segmentation task, the research done by Kitrungrotsakul et al. [82], Kazami et al. [83] and Kitrungrotsakul et al. [84] ranked the top three. The first and third-ranking methods used an ensemble approach where the vesselness probability maps are used as the input making the methods more robust and insensitive to CT intensity changes. Kitrungrotsakul et al. [82] aimed for a patch-wise classification pre-processing step, improving the detection and segmentation of smaller vessels, showing better outcome than Kitrungrotsakul et al. [84]. The second-ranking method [83]followed a multi-task approach using a single encoder and multiple decoders for vessel extraction, center voxel detection and tree construction. This hybrid approach results in accurate extraction and separation of both the hepatic and portal veins.

Regarding classification, the three best algorithms were the following: Mostafiz et al. [85], Hassan et al. [86] and Mitrea et al. [87]. The first [85] and the second [86] highest-ranking methods incorporated computer vision algorithms with DL approaches, as a combined method. In Mostafiz et al. [85], the local binary patterns and Gabor wavelet features are fused with the CNN extracted features, and further classified using a SVM. This work showed as well that the use of edge-preserving modified anisotropic diffusion filtered images as input to the model yielded an improvement of precision in the classification task. The combined strategy using level-set and fuzzy-c-means for segmenting, and auto-encoders for classifying the lesions improved the accuracy of lesion classification in Hassan et al. [86]. Unlike Mostafiz et al. [85] and Hassan et al. [86], the third highest-ranking method introduced by Mitrea et al. [87] for the liver lesion classification tasks utilized a ensembling approach. The probability maps from the different classifiers trained on CEUS and B mode images at the decision level are ensembled, making the model more efficient in classifying the HCC lesions.

And lastly, the best performing models in the detection tasks are Fabijańska et al. [88], Todoroki et al. [89] and Wojciechowska et al. [90]. All three methods used a similar strategy (combined approach) by detecting the lesions from the segmented liver. In Fabijańska et al. [88], and Todoroki et al. [89], the liver is segmented using the computational and statistical shape models respectively whereas the lesions are detected using DNNs. In addition, Fabijańska et al. [88] averaged three phases images to a grayscale MR image and used it as an input which aids in better detection accuracy. Wojciechowska et al. [90] is distinct from the top two methods [88,89] by using DL centered solution to segment the liver, and the combination of intensity thresholding and circularity measure to detect lesions.

9.2. Discussion on architectures

It is worth highlighting the cascade strategy for lesion segmentation. This strategy improves the convergence of the model as well as the generalization of the task, by training each step to tackle tasks following a hierarchical relationship. For instance, the two steps cascade pipeline is preferred by those publications where both the liver and the lesions are segmented. The first model segments the parenchyma, reducing the search space for the second model, in charge of segmenting the lesions. In ([81,108], a model trained to simultaneously segment all the structures are compared to the cascaded approach, hierarchically segmenting structures. In both([81,108], the cascaded approach performs better by reducing the false positives. In [108], the cascaded approach reduces the search space and improves segmentation accuracy even for the smallest structures like vessels. On average, the method achieved a 7.5 % improvement in DICE score per organ using the two-stage hierarchical approach.

In contrast to regular 3D models, the ensemble approach can improve the prediction performance using fewer parameters. This is because the model explores the three orthogonal slices (sagittal, coronal and axial) instead of full volumes. This strategy seems to work well for the vessel segmentation task [82,84]. We also observe similar trend for lesion segmentation tasks in Chlebus et al. [124] and Wang [37]. Chlebus et al. [124] reported the use of ensemble classifier with tri-planar approach yielded a slightly better dice score for both the liver and liver tumor segmentation. In Wang [37], the tri-planar approach reduces the VOE from 8.9 to 6.7 for the liver segmentation and from 16.3 to 13.3 for the lesion segmentation. Similar to tri-planar/multi-planar input, using multiphase (arterial, venous and delayed phase combined) [81,88,133,160] and multi-scale [121,161] input shown to improve the prediction score.

By comparing the evaluation metrics, we realize that the methods using hybrid models and combined approaches are performing well for the liver segmentation and lesion classification tasks. From the experiments reported in the papers reviewed, we observe that using hybrid models can improve the segmentation performance [93] along with faster convergence, overcome the vanishing gradient problem, improve performance [94] and increase the processing speed [114]. The combined approach using the combination of DL models and various computer vision algorithms has also been shown to improve the predictive power compared to standalone DL models or simultaneous approach [77,98]. [77] outperformed U-net (DL only) and other segmentation approaches like active contour, level set, and graph cut. In Guo et al.

[98], their solution has a 1.8 % improvement in DICE score compared to the purely FCN method.

9.3. Discussion on the research lines

The vessel segmentation papers mentioned in the review show a preference toward the segmentation of the whole vascular tree of the liver. Only Yu et al. [147] and Kazami et al. [83], are DL based approaches to segment hepatic and portal veins separately, which is clinically relevant. Being able to differentiate between the hepatic and portal vein system helps the clinician to better understand the structural and volumetric anatomy, especially relevant for treatment planning. Future research should aim to both the segmentation and classification of the three hepatic vascular systems.

Regarding the dimensionality of the input, the 2.5D methods using either tri-planar input or three or five consecutive axial slices as input had better performance both in terms of computational needs and the dice score compared to 2D or 3D approaches [102]. By analyzing a smaller set of neighboring slices, 2.5D is a tradeoff between 2D analysis, with lower computational footprint but only local information, and complete 3D, which provides global information but demands more resources.

Considering the modalities used in these papers, most of them are based on CT images. Very few papers addressed methods focused on MRI, US or laparoscopic videos. In addition to the clinical perspective, the main reason could be the availability of the labeled data which is crucial for training DL models. Publicly available CT labeled datasets for the liver have a major effect on the number of papers published using CT, whereas, for MRI and US, there is a lack of publicly available labeled data. If more labeled datasets would be publicly available for all the modalities, then the algorithms can be tested on multi-modality data which is crucial from the clinical perspective.

Though the DL-based approaches using different methodologies and optimization techniques [186] could improve the prediction performance, still there is a bottleneck concerning the inhomogeneity of the medical images. The developed methods have some limitations when the liver tissue is minimally visible and has high inter-patient variability in liver appearance [99], unable to segment structures in low dose and low contrast images [110], problems in segmenting tumors with fuzzy borders and heterogeneous intensity [131]. To use the developed methods for CAD or treatment planning in clinical routine, the methods developed should be adaptable and reproducible and DL models could be trained with additional varying/ inhomogeneous images.

Due to the clinical importance of image-based analysis of the liver and its lesions and vessels, this review summarizes the existing algorithms and their performance for various image analysis tasks.

10. Future research and directions

From the analysis of the 91 articles included in this review, including methodology, scope and performance, the authors consider of major interest the following research lines:

- Segmentation and classification of the different vascular systems of the liver.
- MRI, US and laparoscopic video are the modalities least researched, because of the availability of data material. Hence, disclose of research data on these image modalities would be of great benefit, enhancing the research on these modalities as well.
- Research on methods to improve robustness against the variability of image quality.
- Promote the use of reference evaluation datasets to better compare the performance of the reported solutions, in a standardized way.

11. Conclusion

From the discussion, incorporating necessary information into the DL models like shape and edge contours, local and global context information, using multi-scale, multi-phase, multi-plane inputs, pre- and post-processing methods will highlight the relevant structures by suppressing the background which can significantly improve the performance.

The DL-based liver lesion segmentation and classification approaches developed so far seem to be promising but we see there is still room for improvement especially to tackle the challenges related to the inhomogeneity of the medical images and the liver structures. To apply the developed methods in clinical use, the researchers should also focus on augmentation techniques to synthetically develop huge variations of realistic labeled medical data which can be further used to train the DL models.

Liver vessel segmentation and classification remain a fairly unexplored research area for DL-based medical image analysis. Current DL-based methods are mainly focused on just segmenting the hepatic vessels as a whole due to the complexity of the vessel structures. Future research should focus on segmenting or classifying the hepatic and portal structures separately which is of high clinical relevance.

Most of the existing research papers focus on liver segmentation from CT scans. However, especially for computer-assisted liver resections, it is very important to have methods capable of multi-modality liver image analysis. This need together with the increasing interest in minimally invasive surgery means we might see an increase in research publications aiming to expand the DL methods onto modalities such as US, MRI or PET. Further research in the domain adaptation and transfer learning networks can address this challenge.

Declaration of competing interest

The authors declare that they have no known competing financial interests or personal relationships that could have appeared to influence the work reported in this paper.

Acknowledgments

This work is supported by H2020-MSCA-ITN Marie Skłodowska-Curie Actions, Innovative Training Networks (ITN) -H2020 MSCA ITN 2016 GA EU project number 722068 High Performance Soft Tissue Navigation (HiPerNav).

Fig. 2 that has been used in the paper is from Orcutt et al. [29] and Figs. 3, 4 and 5 are from radiopaedia.org. The authors would like to acknowledge Orcutt et al. [29] and radiopaedia.org for providing the images as open-source.

Appendix A. Collection of articles surveyed

Table A.1
Articles reviewed on liver segmentation task: S - segmentation, Li - liver parenchyma, MO - multiple organ, Modal - modality, Dim - dimension, DSC - DICE score, ACC - accuracy, VOE - volume overlap error, D1 - dataset 1, D2 - dataset 2, D3 - dataset 3.

Author	Tasks	Method	Modal	Dim	DICE/ACC/VOE	Dataset
Ahmad et al. [91]	LiS	SA	CT	2D	DSC-90.1	SLiver07
Ahmad et al. [92]	LiS	CA	CT	3D	DSC(D1, D2)-(91.83, 94.8)	3DIRCADb, SLiver07
Chung et al. [93]	LiS	HM	CT	3D	DSC-96	SLiver07, 3DIRCADb
Dou et al. [94]	LiS	HM	CT	3D	VOE-5.42	SLiver07
Dou et al. [95]	LiS	CA	CT	3D	VOE-5.37	SLiver07
Fu et al. [96]	MOS	DA	CT	3D	DSC-91.55	Synapse, LiTS
Gibson et al. [97]	LiS	SA	LV	2D	DSC-95	Clinical
Guo et al. [98]	LiS	CA	CT	3D	DSC-95.8	SLiver
Hu et al. [78]	LiS	HM	CT	3D	DSC-97.25	SLiver07, Clinical
Irving et al. [99]	LiS	CA	MR	2D	DSC-95	UK Biobank
Li et al. [76]	LiS	HM	CT, MR	2D	DSC(CT)-98.1, DSC(MR)-93.5	LiTS, CHAOS
Lu et al. [100]	LiS	CA	CT	3D	VOE(D1, D2)-(5.9, 9.36)	Sliver07, 3DIRCADb
Masoumi et al. [101]	LiS	CA	MR	2D	ACC-94	Clinical
Meine et al. [102]	LiS	EC	CT	2D	VOE-5.05	Clinical
Mitta et al. [103]	LiS	CA	MR	3D	DSC-88.1	CHAOS
Mulay et al. [104]	LiS	HM	CT, MR	2D	DSC(CT)-94, DSC(MR)-91	CHAOS
Pandey et al. [105]	LiS	SA	MR	2D	DSC-86.4	CHAOS
Pham et al. [106]	LiS	DA	CT/MR	3D	DSC(D1, D2, D3)-(75.3, 81.7, 69.2)	CHAOS, TCIA, Synapse
Prasad et al. [107]	LiS	SA	CT	2D	DSC-94.5	3DIRCADb
Qin et al. [77]	LiS	CA	CT	2D	DSC-97.3	LiTS
Roth et al. [108]	MOS	CM	CT	3D	DSC-95.4	Clinical
Tang et al. [109]	LiS	DG	CT	2D	VOE(D1,D2)-(8.67, 5.06)	3DIRCADb, SLiver07
Tang et al. [110]	LiS	SA	CT	3D	DSC-94	LiTS, MSD
Wang et al. [111]	LiS	HM	CT, MR	2D	DSC-95	Clinical
Xia et al. [112]	LiS	HM	CT	2D	DSC-97	LiTS, Clinical
P. Xu et al. [113], Z. Xu et al. [68]	LiS	HM	CT	3D	DSC-87.1	LiTS, Clinical
Yang et al. [114]	LiS	HM	CT	3D	DSC-95	Clinical
Yang et al. [115]	LiS	DA	CT/MR	2D	DSC-81	LiTS, Clinical
Yang et al. [116]	LiS	DA	CT/MR	2D	DSC-84.7	LiTS, Clinical
You et al. [117]	LiS	DA	CT/MR	3D	DSC-83.4,	LiTS, Clinical
Zhou et al. [118]	LiS	DA	CT, MR	3D	DSC(CT)-90.3, DSC(MR)91.8	LiTS, CHAOS

Table A.2
Articles reviewed on lesion segmentation task: S - segmentation, Li - liver parenchyma, Le - lesions, Modal - modality, Dim - dimension, DSC - DICE score, VOE - volume overlap error, TPR - true positive rate, D1 - dataset 1, D2 - dataset 2.

Author	Tasks	Method	Modal	Dim	DICE/VOE/TPR	Dataset
Abdalla et al. [79]	LiS, LeS	HM	CT	2.5D	DSC-96.2	LiTS
Bellver et al. [119]	LeS	DG	CT	2.5D	DSC-59	LiTS
Ben-Cohen et al. [120]	LiS, LeS	CM	CT	2.5D	DSC(Li)-89, TPR(Le)-86	SLiver07, Clinical
Bi et al. [121]	LiS, LeS	CM	CT	2D	DSC(Li)-95.9, DSC(Le)-50.01	LiTS
Bi et al. [122]	LeS	EC	CT	2D	DSC-80.71	Clinical
Chlebus et al. [123]	LeS	CM	CT	3D	DSC-65	LiTS
Chlebus et al. [124]	LiS, LeS	EC	MR	2.5D	DSC(Li)-95.1, DSC(Le)-64.7	Clinical
Christ et al. [125]	LiS, LeS	CM	CT	2.5D	DSC(Li)-94.3, DSC(Le)-56	3DIRCADb
Christ et al. [126]	LiS, LeS	CM	CT, MR	2.5D	DSC(Li)-87, DSC(Le)-69.7	3DIRCADb, Clinical
Han [127]	LeS	HM	CT	2.5D	DSC-67	LiTS
Hoogi et al. [128]	LeS	DG	CT	3D	DSC-71	Clinical
Jiang et al. [129]	LeS	HM	CT	3D	DSC(Li)-94.5, DSC(Le)-62	LiTS, 3DIRCADb
Jiao et al. [80]	LeS	CM	CT	2.5D	DSC-96	TCGA-LIHC
Kaluva et al. [130]	LiS, LeS	CM	CT	2D	DSC(Li)-92.3, DSC(Le)-62.5	LiTS
Li et al. [131]	LeS	SA	CT	2D	DSC-82.64	Clinical
Li et al. [132]	LiS, LeS	HM	CT	3D	DSC(Li)-96.1, DSC(Le)-68.6	LiTS, 3DIRCADb
Ouhmich et al. [81]	LiS, LeS	CM	CT	2D	DSC(Li)-89.9, DSC(Le)-90.5	Clinical
Sun et al. [133]	LeS	EC	CT	2D	VOE(D1)-8.1, VOE(D2)-4.5	3DIRCADb, Clinical
Tian et al. [134]	LiS, LeS	HM	CT	2D	DSC(Li)-94.2, DSC(Le)-54.9	LiTS
Vivanti et al. [135]	LeS	AR	CT	3D	VOE-16.15	Clinical
Vivanti et al. [136]	LeS	AR	CT	3D	TPR-86	Clinical
Vorontsov et al. [137]	LiS, LeS	CM	CT	2D	DSC(Li)-95.1, DSC(Le)-66.1	LiTS
Wang [37]	LiS, LeS	EC	CT	3D	VOE(Li)-6.7, VOE(Le)-13.3	3DIRCADb
Zheng et al. [138]	LeS	CA	CT	2D	VOE-17	LiTS, 3DIRCADb

Table A.3
Articles reviewed on vessel segmentation task: S - segmentation, Ve - vessels, HV - hepatic vein, PV - portal vein, Modal - modality, Dim - dimension, DSC - DICE score, ACC - accuracy, IoU - intersection over union.

Author	Tasks	Method	Modal	Dim	DICE/ACC/IoU	Dataset
Huang et al. [139]	VeS	SA	CT	2D	DSC-67.5	SLiver07, 3DIRCADb
Ibragimov et al. [140]	VeS	CA	CT	2D	DSC-83	Clinical
Kazami et al. [83]	VeS	SA	CT	3D	DSC(HV)-90, DSC(PV)-94	Clinical
Kitrungrotsakul et al. [141]	VeS	EC	CT	3D	DSC-83	Clinical
Kitrungrotsakul et al. [84]	VeS	EC	CT	3D	DSC-87.9	Clinical
Kitrungrotsakul et al. [82]	VeS	EC	CT	2D	DSC-96	3DIRCAD, VascuSynth
Mishra et al. [142]	VeS	HM	US	2D	DSC-79,IoU-83	Clinical
Mishra et al. [143]	VeS	CA	US	2D	ACC-99.14, IoU-69.62	Clinical
Survarachakan et al. [144]	VeS	EC	CT	3D	DSC-81.8	Clinical
Thomson et al. [145]	Ves	SA	US	3D	DSC-74(3D), DSC-78(2D)	Clinical
Yan et al. [146]	VeS	HM	CT	3D	DSC-80.5	3DIRCADb, Clinical
Yu et al. [147]	VeS	HM	CT	3D	DSC(HV)-71.7, DSC(PV)-76.5	Clinical

Table A.4
Articles reviewed on lesion classification task: C - classification, D - detection, Le - lesions, Modal - modality, Dim - dimension, DSC - DICE score, ACC - accuracy, AUC - area under curve, RA - (ROC-AUC).

Author	Tasks	Method	Modal	Dim	DICE/ACC/AUC/RA	Dataset
Ben-Cohen et al. [148]	LeC	SA	CT	2D	ACC-80	Clinical
Căleanu et al. [149]	LeC	SA	US	2D	ACC-88	Clinical
Hassan et al. [86]	LeC	CA	US	2D	ACC-97.2	Clinical
Liang et al. [150]	LeC	HM	CT	2D	ACC-87.58	Clinical
Liang et al. [151]	LeC	HM	CT	2D	ACC-90.93	Clinical
Marya et al. [152]	LeC	SA	US	2D, 3D	AUC-0.86(2D), 0.904(3D)	clinical
Meng et al. [153]	LeC	HM	CT	2D	ACC-96.08	Clinical
Mitrea et al. [87]	LeC	EC	US	2D	ACC-97	Clinical
Mostafiz et al. [85]	LeC	CA	US	2D	ACC-98.4	Clinical
Pan et al. [154]	LeC	SA	US	3D	ACC-93.1	Clinical
Romero et al. [155]	LeC	HM	CT	2.5D	ACC-96	UK Biobank
Schmauch et al. [156]	LeD, LeC	SA	US	2D	RA(D)-93.5, RA(C)-91.6	JFR18
Sîrbu et al. [157]	LeC	SA	US	3D	ACC-95.71	Clinical
Trivizakis et al. [158]	LeC	SA	MR	3D	ACC-83	Clinical
Wu et al. [159]	LeC	CA	US	2D	ACC-86.36	Clinical
Yasaka et al. [160]	LeC	SA	CT	2D	ACC-84	Clinical
Zhang et al. [161]	LeC	SA	MR	3D	DSC-80	Clinical

Table A.5
Articles reviewed on lesion detection task: S - Segmentation, D - detection, Li - liver parenchyma, Le - lesions, Modal - modality, Dim - dimension, DSC - DICE score, ACC - accuracy, TPR - true positive rate, SEN - sensitivity.

Author	Tasks	Method	Modal	Dim	DICE/ACC/SEN/TPR	Dataset
Bousabarah et al. [162]	LiS, LeD	AR	MR	2D	DSC(LiS)-91, DSC(LeD)-68	Clinical
Fabijańska et al. [88]	LeD	CA	MR	2D	ACC-98.5	Clinical
Frid-Adar et al. [163]	LeD	SA	CT	2D	TPR-86.8	Clinical
Jansen et al. [164]	LiS, LeD	AR	CT, MR	2.5D	DSC(Li)-94, SEN(Le)-99.8	Clinical
Lee et al. [165]	LeD	AR	CT	2.5D	SEN-93.88	Clinical
Todoroki et al. [89]	LeD	CA	CT	2D	ACC-84	Clinical
Wojciechowska et al. [90]	LeD	CA	MR	2D	ACC-83	UK BioBank

References

[1] Sung H, Ferlay J, Siegel RL, Laversanne M, Soerjomataram I, Jemal A, Bray F. Global cancer statistics 2020: Globocan estimates of incidence and mortality worldwide for 36 cancers in 185 countries. URL: CA Cancer J Clin 2021;71: 209–49. https://doi.org/10.3322/caac.21660. https://acsjournals.onlinelibrary.wiley.com/doi/abs/10.3322/caac.21660.

[2] Ferlay J, Shin HR, Bray F, Forman D, Mathers C, Maxwell Parkin D. Estimates of worldwide burden of cancer in 2008: globocan. International journal of cancer. J Int Cancer 2010;127:2893–917. https://doi.org/10.1002/ijc.25516.

[3] Heimann T, van Ginneken B, Styner M, Arzhaeva Y, Aurich V, Bauer C, Beck A, Becker C, Beichel R, Bekes G, Bello F, Binnig G, Bischof H, Bornik A, M M Cashman P, Chi Y, Cordova A, Dawant BM, Fidrich M, Wolf I. Comparison and evaluation of methods for liver segmentation from ct datasets. IEEE Trans Med Imaging 2009;28:1251–65. https://doi.org/10.1109/TMI.2009.2013851.

[4] Domingo J, Dura E, Göçeri E. Iteratively learning a liver segmentation using probabilistic atlases: preliminary results. In: 2016 15th IEEE international conference on machine learning and applications (ICMLA); 2016. p. 593–8. https://doi.org/10.1109/ICMLA.2016.0104.

[5] Dura E, Domingo J, Ayala G, Marti-Bonmati L, Goceri E. Probabilistic atlas construction. Biomed Eng Online 2017;16. https://doi.org/10.1186/s12938-016-0305-8.

[6] Dura E, Domingo J, Goceri E, Marti-Bonmati L. A method for liver segmentation in perfusion mr images using probabilistic atlases and viscous reconstruction. Pattern Anal Applic 2017;21. https://doi.org/10.1007/s10044-017-0666-z.

[7] Goceri E. A comparative evaluation for liver segmentation from spir imagesand a novel level set method using signed pressure force function. https://core.ac.uk/reader/324140990; 2013.

[8] Goceri E. Automatic labeling of portal and hepatic veins from mr images prior to liver transplantation. Int J Comput Assist Radiol Surg 2016;11. https://doi.org/10.1007/s11548-016-1446-8.

[9] Goceri E, Unlu MZ, Guzelis C, Dicle O. An automatic level set based liver segmentation from mri data sets. In: 2012 3rd international conference on image processing theory, tools and applications (IPTA); 2012. p. 192–7.

[10] Campadelli P, Casiraghi E, Esposito A. Liver segmentation from computed tomography scans: a survey and a new algorithm. Artif Intell Med 2009;45:185–96. https://doi.org/10.1016/j.artmed.2008.07.020. computational Intelligence and Machine Learning in Bioinformatics.

[11] Mharib AM, Ramli AR, Mashohor S, Mahmood RB. Survey on liver ct image segmentation methods. Artif Intell Rev 2012;37:83–95. https://doi.org/10.1007/s10462-011-9220-3.

[12] Moghbel M, Mashohor S, Mahmud R, Saripan M. Review of liver segmentation and computer assisted detection/diagnosis methods in computed tomography. Artif Intell Rev 2018;50. https://doi.org/10.1007/s10462-017-9550-x.

[13] Priyadarsini S, Selvathi D. Survey on segmentation of liver from ct images. In: 2012 IEEE international conference on advanced communication control and computing technologies (ICACCCT); 2012. p. 234–8. https://doi.org/10.1109/ICACCCT.2012.6320777.

[14] Punia R, Singh SK. Review on machine learning techniques for automatic segmentation of liver images. In: International journal of advanced research in computer science and software engineering; 2013. p. 666–70.

[15] Rathore S, Iftikhar MA, Hussain M, Jalil A. Texture analysis for liver segmentation and classification: a survey. Front Inf Technol 2011;2011:121–6.

[16] Ginneken BV, Heimann T, Styner M. M.: 3d segmentation in the clinic: a grand challenge. In: MICCAI workshop on 3D segmentation in the clinic: a grand challenge. 2007; 2007. p. 7–15.

[17] Deng X, Du G. 3d liver tumor segmentation challenge 2008. In: MICCAI workshop; 2008. abs/1702.05970.

[18] Bilic P, Christ PF, Vorontsov E, Chlebus G, Chen H, Dou Q, Fu C, Han X, Heng P, Hesser J, Kadoury S, Konopczynski TK, Le M, Li C, Li X, Lowengrub JS, Meine H, Moltz JH, Pal C, Piraud M, Qi X, Qi J, Rempfler M, Roth K, Schenk A, Lipková J, Sekuboyina A, Zhou P, Hülsemeyer C, Beetz M, Ettlinger F, Grün F, Kaissis G, Lohöfer F, Braren R, Holch J, Hofmann F, Sommer WH, Heinemann V, Jacobs C, Mamani GEH, van Ginneken B, Chartrand G, Tang A, Drozdzal M, Ben-Cohen A, Klang E, Amitai MM, Konen E, Greenspan H, Moreau J, Hostettler A, Soler L, Vivanti R, Szeskin A, Lev-Cohain N, Sosna J, Joskowicz L, Menze BH. The liver tumor segmentation benchmark (lits). CoRR; 2019.

[19] Anaya-Isaza A, Mera-Jiménez L, Zequera-Diaz M. An overview of deep learning in medical imaging. URL Inf Med 2021;26:100723. https://doi.org/10.1016/j.imu.2021.100723. https://www.sciencedirect.com/science/article/pii/S2352914821002033.

[20] Anteby R, Klang E, Horesh N, Nachmany I, Shimon O, Barash Y, Kopylov U, Soffer S. Deep learning for noninvasive liver fibrosis classification: a systematic review. Liver Int 2021;41. https://doi.org/10.1111/liv.14966.

[21] Azer S. Deep learning with convolutional neural networks for identification of liver masses and hepatocellular carcinoma: a systematic review. J Gastrointest Oncol 2019;11:1218–30. https://doi.org/10.4251/wjgo.v11.i12.1218.

[22] Khorsandi S, Hardgrave H, Osborn T, Klutts G, Nigh J, Spencer-Cole R, Kakos C, Anastasiou I, Mavros M, Giorgakis E. Artificial intelligence in liver transplantation. Transplant Proc 2021;53:2939–44. https://doi.org/10.1016/j.transproceed.2021.09.045. publisher Copyright: © 2021 Elsevier Inc.

[23] Liu S, Wang Y, Yang X, Lei B, Liu L, Li SX, Ni D, Wang T. Deep learning in medical ultrasound analysis: a review. Engineering 2019;5:261–75. https://doi.org/10.1016/j.eng.2018.11.020. https://www.sciencedirect.com/science/article/pii/S2095809918301887.

[24] Song K. Current status of deep learning applications in abdominal ultrasonography. Ultrasonography 2020;40. https://doi.org/10.14366/usg.20085.

[25] Sosna J. Deep learning for automated normal liver volume estimation. Radiology 2021. https://doi.org/10.1148/radiol.2021212010.

[26] Zhou L, Wang J, Yuan Yu S, Wu GG, Wei Q, Deng Y, Wu X, Cui X, Dietrich C. Artificial intelligence in medical imaging of the liver. World J Gastroenterol 2019;25:672–82.

[27] Betts JG, Youg KA, Wise JA, Johnson E, Poe B, Kruse DH, Korol O, Johnson JE, Womble M, DeSaix P. Anatomy and physiology. chapter 23. URL: OpenStax; 2013. https://openstax.org/details/books/anatomy-and-physiology.

[28] Lorente S, Hautefeuille M, Sanchez-Cedillo A. The liver, a functionalized vascular structure. Sci Rep 2020;10:1–10. https://doi.org/10.1038/s41598-020-73208-8.

[29] Orcutt ST, Kobayashi K, Sultenfuss M, Hailey BS, Sparks A, Satpathy B, Anaya DA. Portal vein embolization as an oncosurgical strategy prior to major hepatic resection: anatomic, surgical, and technical considerations. Front Surg 2016;3:14. https://doi.org/10.3389/fsurg.2016.00014.

[30] Couinaud L. Le Foie-Etudes Anatomiques et Chirurgicales1957. Paris: Masson & Cie; 1957.

[31] Bismuth H. Surgical anatomy and anatomical surgery of the liver. World J Surg 1982;6:3–9. https://doi.org/10.1007/BF01656368.

[32] Hennedige T, Venkatesh S. Imaging of hepatocellular carcinoma: diagnosis, staging and treatment monitoring. Cancer Imaging 2013;12:530–47. https://doi.org/10.1102/1470-7330.2012.0044.

[33] Asemota J, Saleh M, Igbinovia O, Burns D. A concise review on current trends in imaging and surgical management of hepatocellular carcinoma. URL: Cureus 2020;12:9191. https://doi.org/10.7759/cureus.9191. https://www.ncbi.nlm.nih.gov/pmc/articles/PMC7426666/.

[34] Hussain SM, Semelka RC. Hepatic imaging: comparison of modalities. URL: Radiol Clin N Am 2005;43:929–47. https://doi.org/10.1016/j.rcl.2005.05.006. https://linkinghub.elsevier.com/retrieve/pii/S0033838905000941.

[35] Oliva MR, Saini S. Liver cancer imaging: role of CT, MRI, US and PET. Cancer Imaging 2004;4. https://doi.org/10.1102/1470-7330.2004.0011. S42–S46. URL: /pmc/articles/PMC1435346//pmc/articles/PMC1435346/?report=abstracthttps://www.ncbi.nlm.nih.gov/pmc/articles/PMC1435346/.

[36] Schraml C, Kaufmann S, Rempp H, Syha R, Ketelsen D, Notohamiprodjo M, Nikolaou K. Imaging of HCC—current state of the art. URL: Diagnostics 2015;5:513–45. https://doi.org/10.3390/diagnostics5040513. https://www.mdpi.com/2075-4418/5/4/513/htmhttps://www.mdpi.com/2075-4418/5/4/513http://www.mdpi.com/2075-4418/5/4/513.

[37] Wang G, Zhu S, Li X. Comparison of values of CT and MRI imaging in the diagnosis of hepatocellular carcinoma and analysis of prognostic factors. URL: Oncol Lett 2018;17:1184–8. https://doi.org/10.3892/ol.2018.9690. http://www.spandidos-publications.com/10.3892/ol.2018.9690/abstracthttps://www.spandidos-publications.com/10.3892/ol.2018.9690http://www.spandidos-publications.com/10.3892/ol.2018.9690.

[38] Floriani I, Torri V, Rulli E, Garavaglia D, Compagnoni A, Salvolini L, Giovagnoni A. Performance of imaging modalities in diagnosis of liver metastases from colorectal cancer: a systematic review and meta-analysis. URL: J Magn Reson Imaging 2010;31:19–31. https://doi.org/10.1002/jmri.22010. https://pubmed.ncbi.nlm.nih.gov/20027569/https://onlinelibrary.wiley.com/doi/10.1002/jmri.22010.

[39] Miller F, Hammond N, Siddiqi A, Shroff S, Khatri G, Wang Y, Merrick L, Nikolaidis P. Utility of diffusion-weighted mri in distinguishing benign and malignant hepatic lesions. J Magn Reson Imaging 2010;32:138–47. https://doi.org/10.1002/jmri.22235.

[40] Vilgrain V, Esvan M, Ronot M, Caumont-Prim A, Aubé C, Chatellier G. A meta-analysis of diffusion-weighted and gadoxetic acid-enhanced mr imaging for the detection of liver metastases. Eur Radiol 2016;26:4595–615.

[41] Zhang R, Mergo P, Sistrom C, Torres G. Assessment of combined superparamagnetic iron oxide and dynamic gadolinium-enhanced mri of focal hepatic lesions. In: Radiology, radiological Soc north Amer 20th and northampton Sts, Easton, PA 18042 USA; 2000. p. 278–9.

[42] Sun B, Lv Y, Xing D, Li J. Imaging performance and clinical value of contrast-enhanced ultrasonography and computed tomography in the diagnosis of liver cancer. Oncol Lett 2018;15:7669. https://doi.org/10.3892/ol.2018.8281. URL: /pmc/articles/PMC5934724//pmc/articles/PMC5934724/?report=abstracthttps://www.ncbi.nlm.nih.gov/pmc/articles/PMC5934724/http://www.spandidos-publications.com/10.3892/ol.2018.8281.

[43] Bartolotta T, Taibbi A, Midiri M, Lagalla R. Focal liver lesions: contrast-enhanced ultrasound. Abdom Imaging 2008;34:193–209. https://doi.org/10.1007/s00261-008-9378-6.

[44] Barr R, Ferraioli G, Palmeri M, Goodman ZD, Garcia-Tsao G, Rubin J, Garra B, Myers RP, Wilson S, Rubens D, Levine D. Elastography assessment of liver fibrosis: society of radiologists in ultrasound consensus conference statement. Ultrasound Q 2016;32:94–107. https://doi.org/10.1097/RUQ.0000000000000209.

[45] D'Onofrio M, Crosara S, De Robertis R, Canestrini S, Demozzi E, Gallotti A, Pozzi Mucelli R. Acoustic radiation force impulse of the liver. World J Gastroenterol 2013;19:4841–9. https://doi.org/10.3748/wjg.v19.i30.4841.

[46] Biswas M, Kuppili V, Edla DR, Suri HS, Saba L, Marinhoe RT, Sanches JM, Suri JS. Symtosis: a liver ultrasound tissue characterization and risk stratification in optimized deep learning paradigm. Comput Methods Programs Biomed 2018;155:165–77.

[47] Byra M, Styczynski G, Szmigielski C, Kalinowski P, Michałowski Ł, Paluszkiewicz R, Ziarkiewicz-Wróblewska B, Zieniewicz K, Sobieraj P, Nowicki A. Transfer learning with deep convolutional neural network for liver steatosis assessment in ultrasound images. Int J Comput Assist Radiol Surg 2018;13:1895–903.

[48] Liu X, Song JL, Wang SH, Zhao JW, Chen YQ. Learning to diagnose cirrhosis with liver capsule guided ultrasound image classification. Sensors 2017;17:149.

[49] Vernuccio F, Cannella R, Bartolotta TV, Galia M, Tang A, Brancatelli G. Advances in liver us, ct, and mri: moving toward the future. Eur Radiol Exp 2021;5:1–16.

[50] Paolucci I, Schwalbe M, Prevost GA, Lachenmayer A, Candinas D, Weber S, Tinguely P. Design and implementation of an electromagnetic ultrasound-based navigation technique for laparoscopic ablation of liver tumors. URL: Surg Endosc 2018;32:3410–9. https://doi.org/10.1007/s00464-018-6088-1. https://pubmed.ncbi.nlm.nih.gov/29435744/http://link.springer.com/10.1007/s00464-018-6088-1.

[51] Reinacher PC, Velthoven V. Intraoperative ultrasound imaging: practical applicability as a real-time navigation system. URL:. In: Acta neurochirurgica. Supplement. Acta Neurochir Suppl. volume 85; 2003. p. 89–93. https://doi.org/10.1007/978-3-7091-6043-5_12. https://pubmed.ncbi.nlm.nih.gov/12570142/http://link.springer.com/10.1007/978-3-7091-6043-5_12.

[52] Berazaluce AMC, Hanke RE, von Allmen D, Racadio JM. The state of the hybrid operating room: technological acceleration at the pinnacle of collaboration. Curr Surg Rep 2019;7:1–12. https://doi.org/10.1007/S40137-019-0229-X. https://link.springer.com/article/10.1007/s40137-019-0229-x.

[53] Lencioni R, Cioni D, Crocetti L, Bartolozzi C. Percutaneous ablation of hepatocellular carcinoma: state-of-the-art. S91–S97. URL: Liver Transpl 2004;10. https://doi.org/10.1002/lt.20043. https://onlinelibrary.wiley.com/doi/10.1002/lt.20043.

[54] Nault JC, Sutter O, Nahon P, Ganne-Carrié N, Séror O. Percutaneous treatment of hepatocellular carcinoma: state of the art and innovations. J Hepatol 2018;68:783–97. https://doi.org/10.1016/j.jhep.2017.10.004. revision #91189, https://linkinghub.elsevier.com/retrieve/pii/S0168827817323516.

[55] For Energy ECDG. Medical radiation exposure of the European population. URL: https://data.europa.eu/doi/10.2833/708119; 2015. https://doi.org/10.2833/708119.

[56] Masjedi H, Zare MH, Keshavarz Siahpoush N, Razavi-Ratki SK, Alavi F, Shabani M. European trends in radiology: investigating factors affecting the number of examinations and the effective dose. URL: Radiol Med 2020;125:296–305. https://doi.org/10.1007/s11547-019-01109-6. https://link.springer.com/article/10.1007/s11547-019-01109-6http://link.springer.com/10.1007/s11547-019-01109-6.

[57] Eurostat. Health in the European Union – facts and figures. URL:. 2020.

[58] OECD. Health at a Glance 2019: OECD indicators. Health at a glance. OECD Publishing; 2019. https://doi.org/10.1787/4dd50c09-en. https://www.oecd-ilibrary.org/social-issues-migration-health/health-at-a-glance-2003_health_glance-2003-enhttps://www.oecd-ilibrary.org/social-issues-migration-health/health-at-a-glance-2019_4dd50c09-en.

[59] Hong AS, Levin D, Parker L, Rao VM, Ross-Degnan D, Wharam JF. Trends in diagnostic imaging utilization among medicare and commercially insured adults from 2003 through 2016. Radiology 2020;294:342–50. https://doi.org/10.1148/radiol.2019191116. https://pubs.rsna.org/doi/abs/10.1148/radiol.2019191116http://pubs.rsna.org/doi/10.1148/radiol.2019191116.

[60] Yao X. Evolving artificial neural networks. Proc IEEE 1999;87:1423–47.

[61] LeCun Y, Boser B, Denker J, Henderson D, Howard R, Hubbard W, Jackel L. Handwritten digit recognition with a back-propagation network. In: Touretzky D, editor. Advances in neural information processing systems. Morgan-Kaufmann; 1990. p. 396–404.

[62] Lecun Y, Boser B, Denker J, Henderson D, Howard RE, Hubbard W, Jackel L. Backpropagation applied to handwritten zip code recognition. Neural Comput 1989;1:541–51. https://doi.org/10.1162/neco.1989.1.4.541.

[63] Goodfellow I, Bengio Y, Courville A. Deep learning. MIT Press; 2016.

[64] Hinton GE. Deep belief networks. Scholarpedia 2009;4:5947. https://doi.org/10.4249/scholarpedia.5947. revision #91189.

[65] Goodfellow I, Pouget-Abadie J, Mirza M, Xu B, Warde-Farley D, Ozair S, Courville A, Bengio Y. Generative adversarial nets. In: Ghahramani Z, Cortes C, Lawrence ND, Welling M, Weinberger KQ, editors. Advances in Neural Information Processing Systems. 27. Curran Associates, Inc; 2014. p. 2672–80.

[66] Kavur AE, Selver MA, Dicle O, Barıs¸ M, Gezer NS. CHAOS - combined (CT-MR) healthy abdominal organ segmentation challenge data. 2019. https://doi.org/10.5281/zenodo.3362844.

[67] Antonelli M, Reinke A, Bakas S, Farahani K, AnnetteKopp-Schneider, Landman BA, Litjens G, Menze B, Ronneberger O, Summers RM, van Ginneken B, Bilello M, Bilic P, Christ PF, Do RKG, Gollub MJ, Heckers SH, Huisman H, Jarnagin WR, McHugo MK, Napel S, Pernicka JSG, Rhode K, Tobon-Gomez C, Vorontsov E, Huisman H, Meakin JA, Ourselin S, Arbelaez P, Bae B, Chen S, Daza L, Feng J, He B, Isensee F, Ji Y, Jia F, Kim N, Kim I, Merhof D, Pai A, Park B, Perslev M, Rezaiifar R, Rippel O, Sarasua I, Shen W, Son J, Wachinger C, Wang L, Wang Y, Xia Y, Xu D, Xu Z, Zheng Y, Simpson AL, Maier-Hein L, Cardoso MJ, Wiesenfarth M. The medical segmentation decathlon. arXiv:2106.05735; 2021.

[68] Xu Z, Lu D, Wang Y, Luo J, Jagadeesan J, Ma K, Zheng Y, Li X. Noisy labels are treasure: mean-teacher-assisted confident learning for hepatic vessel segmentation. arXiv preprint; 2021. arXiv:2106.01860.

[69] Soler L, Hostettler A, Agnus V, Charnoz A, Moreau JBFJ, Osswald AB, Bouhadjar M, Marescaux J. 3d image reconstruction for comparison of algorithm database: a patient-specific anatomical and medical image database. 2012.

[70] Taha AA, Hanbury A. Metrics for evaluating 3D medical image segmentation: analysis, selection, and tool. BMC Med Imaging 2015;15:29.

[71] Belogay E, Cabrelli C, Molter U, Shonkwiler R. Calculating the Hausdorff distance between curves. URL: Inf Process Lett 1997;64:17–22. https://doi.org/10.1016/S0020-0190(97)00140-3. https://linkinghub.elsevier.com/retrieve/pii/S0020019097001403.

[72] Rote G. Computing the minimum Hausdorff distance between two point sets on a line under translation. URL: Inf Process Lett 1991;38:123–7. https://doi.org/10.1016/0020-0190(91)90233-8. https://linkinghub.elsevier.com/retrieve/pii/0020019091902338.

[73] Jiang Z, Ding C, Liu M, Tao D. Two-stage cascaded UNet: 1st place solution to BraTS challenge 2019 segmentation task. URL:. In: volume 11992. Springer; 2020. p. 231–41. https://doi.org/10.1007/978-3-030-46640-4{_}22. https://link.springer.com/chapter/10.1007/978-3-030-46640-4_22http://link.springer.com/10.1007/978-3-030-46640-4_22.

[74] Raudaschl PF, Zaffino P, Sharp GC, Spadea MF, Chen A, Dawant BM, Albrecht T, Gass T, Langguth C, Lüthi M, Jung F, Knapp O, Wesarg S, Mannion-Haworth R, Bowes M, Ashman A, Guillard G, Brett A, Vincent G, Orbes-Arteaga M, Cárdenas-Peña D, Castellanos-Dominguez G, Aghdasi N, Li Y, Berens A, Moe K, Hannaford B, Schubert R, Fritscher KD. Evaluation of segmentation methods on head and neck CT: auto-segmentation challenge 2015. URL: Med Phys 2017;44:2020–36. https://doi.org/10.1002/mp.12197. http://doi.wiley.com/10.1002/mp.12197.

[75] Fawcett T. An introduction to roc analysis. URL: Pattern Recogn Lett 2006;27:861–74. https://doi.org/10.1016/j.patrec.2005.10.010. https://www.sciencedirect.com/science/article/pii/S016786550500303X.

[76] Li C, Tan Y, Chen W, Luo X, He Y, Gao Y, Li F. Anu-net: attention-based nested u-net to exploit full resolution features for medical image segmentation. URL: Comput Graph 2020;90:11–20. https://doi.org/10.1016/j.cag.2020.05.003. https://www.sciencedirect.com/science/article/pii/S0097849320300546.

[77] Qin W, Wu J, Han F, Yuan Y, Zhao W, Ibragimov B, Gu J, Xing L. Superpixel-based and boundary-sensitive convolutional neural network for automated liver segmentation. Phys Med Biol 2018;63:095017.

[78] Hu P, Wu F, Peng J, Liang P, Kong D. Automatic 3d liver segmentation based on deep learning and globally optimized surface evolution. Phys Med Biol 2016;61:8676.

[79] Abdalla A, Ahmed N, Dakua S, Balakrishnan S, Abinahed J. A surgical-oriented liver segmentation approach using deep learning. In: 2020 IEEE international conference on informatics, IoT, and enabling technologies (ICIoT); 2020. p. 318–22. https://doi.org/10.1109/ICIoT48696.2020.9089512.

[80] Jiao Q, Li Z, Song S. Ct image segmentation of liver tumor based on improved convolution neural network. DEStech Trans Comput Sci Eng 2019. https://doi.org/10.12783/dtcse/cisnrc2019/33333.

[81] Ouhmich F, Agnus V, Noblet V, Heitz F, Pessaux P. Liver tissue segmentation in multiphase ct scans using cascaded convolutional neural networks. Int J Comput Assist Radiol Surg 2019. https://doi.org/10.1007/s11548-019-01989-z.

[82] Kitrungrotsakul T, Han XH, Iwamoto Y, Lin L, Foruzan A, Xiong W, Chen YW. Vessel net: a deep convolutional neural network with multi pathways for robust hepatic vessel segmentation. Comput Med Imaging Graph 2019;75. https://doi.org/10.1016/j.compmedimag.2019.05.002.

[83] Kazami Y, Kaneko J, Keshwani D, Takahashi R, Kawaguchi Y, Ichida A, Ishizawa T, Akamatsu N, Arita J, Hasegawa K. Artificial intelligence enhances the accuracy of portal and hepatic vein extraction in computed tomography for virtual hepatectomy. J Hepatobiliary Pancreat Sci 2021. https://doi.org/10.1002/jhbp.1080.

[84] Kitrungrotsakul T, Han XH, Wei X, Chen YW. Multi-pathways cnn for robust vascular segmentation. In: Medical imaging 2018: biomedical applications in molecular, structural, and functional imaging. International Society for Optics and Photonics; 2018. 105781S.

[85] Mostafiz R, Rahman MM, Islam A, Belkasim S. Focal liver lesion detection in ultrasound image using deep feature fusions and super resolution. Mach Learn Knowl Extraction 2020;2:172–91.

[86] Hassan TM, Elmogy M, Sallam ES. Diagnosis of focal liver diseases based on deep learning technique for ultrasound images. Arab J Sci Eng 2017;42:3127–40.

[87] Mitrea D, Badea R, Mitrea P, Brad S, Nedevschi S. Hepatocellular carcinoma automatic diagnosis within ceus and b-mode ultrasound images using advanced machine learning methods. Sensors 2021:21. https://doi.org/10.3390/s21062202. https://www.mdpi.com/1424-8220/21/6/2202.

[88] Fabijańska A, Vacavant A, Lebre MA, Pavan ALM, de Pina DR, Abergel A, Chabrot P, Magnin B. U-catchcc: an accurate hcc detector in hepatic dce-mri sequences based on an u-net framework. In: Chmielewski LJ, Kozera R, Orłowski A, Wojciechowski K, Bruckstein AM, Petkov N, editors. Computer vision and graphics. Cham: Springer International Publishing; 2018. p. 319–28.

[89] Todoroki Y, Han XH, Iwamoto Y, Lin L, Hu H, Chen YW. Detection of liver tumor candidates from ct images using deep convolutional neural networks. In: International conference on innovation in medicine and healthcare. Springer; 2017. p. 140–5.

[90] Wojciechowska M, Irving B, Dennis A, Wilman HR, Banerjee R, Brady SM, Kelly M. Automated detection of cystic lesions in quantitative t1 liver images. In: Nixon M, Mahmoodi S, Zwiggelaar R, editors. Medical image understanding and analysis. Cham: Springer International Publishing; 2018. p. 51–6.

[91] Ahmad M, Yang J, Ai D, Qadri SF, Wang Y. Deep-stacked auto encoder for liver segmentation. In: Chinese conference on image and graphics technologies. Springer; 2017. p. 243–51.

[92] Ahmad M, Ai D, Xie G, Furqan Qadri S, Song H, Huang Y, Wang Y, Yang J. Deep belief network modeling for automatic liver segmentation. URL: IEEE Access 2019. https://doi.org/10.1109/ACCESS.2019.2896961.

[93] Chung M, Lee J, Lee M, Lee J, Shin Y. Deeply self-supervising edge-to-contour neural network applied to liver segmentation. CoRR; 2018. abs/1505.04597. arXiv:1505.04597.

[94] Dou Q, Chen H, Jin Y, Yu L, Qin J, Heng PA. 3d deeply supervised network for automatic liver segmentation from ct volumes. In: International conference on medical image computing and computer-assisted intervention. Springer; 2016. p. 149–57.

[95] Dou Q, Yu L, Chen H, Jin Y, Yang X, Qin J, Heng PA. 3d deeply supervised network for automated segmentation of volumetric medical images. Med Image Anal 2017;41:40–54.

[96] Fu S, Lu Y, Wang Y, Zhou Y, Shen W, Fishman E, Yuille A. Domain adaptive relational reasoning for 3d multi-organ segmentation. arXiv:2005.09120; 2020.

[97] Gibson E, Robu MR, Thompson S, Edwards PE, Schneider C, Gurusamy K, Davidson B, Hawkes DJ, Barratt DC, Clarkson MJ. Deep residual networks for automatic segmentation of laparoscopic videos of the liver. In: Medical imaging 2017: image-guided procedures, robotic interventions, and modeling. International Society for Optics and Photonics; 2017. 101351M.

[98] Guo X, Schwartz LH, Zhao B. Automatic liver segmentation by integrating fully convolutional networks into active contour models. Med Phys 2019;46(10):4455–69.

[99] Irving B, Hutton C, Dennis A, Vikal S, Mavar M, Kelly M, Brady JM. Deep quantitative liver segmentation and vessel exclusion to assist in liver assessment. In: Annual conference on medical image understanding and analysis. Springer; 2017. p. 663–73.

[100] Lu F, Wu F, Hu P, Peng Z, Kong D. Automatic 3d liver location and segmentation via convolutional neural network and graph cut. Int J Comput Assist Radiol Surg 2017;12:171–82.

[101] Masoumi H, Behrad A, Pourmina MA, Roosta A. Automatic liver segmentation in mri images using an iterative watershed algorithm and artificial neural network. Biomed Signal Process Control 2012;7:429–37.

[102] Meine H, Chlebus G, Ghafoorian M, Endo I, Schenk A. Comparison of u-net-based convolutional neural networks for liver segmentation in CT. CoRR; 2018. abs/1810.04017. arXiv:1810.04017.
[103] Mitta D, Chatterjee S, Speck O, Nurnberger A. Upgraded w-net with attention gates and its application in unsupervised 3d liver segmentation. In: Proceedings of the 10th international conference on pattern recognition applications and methods; 2021. https://doi.org/10.5220/0010221504880494. URL: doi: 10.5220/0010221504880494.
[104] Mulay S, Deepika G, Jeevakala S, Ram K, Sivaprakasam M. Liver segmentation from multimodal images using hed-mask r-cnn. In: International workshop on multiscale multimodal medical imaging. Springer; 2019. p. 68–75.
[105] Pandey P, Pai A, Bhatt N, Das P, Makharia G, AP P, Mausam. Contrastive semi-supervised learning for 2d medical image segmentation. abs/2106.06801. URL:; 2021 CoRR; 2021. arXiv:2106.06801, https://arxiv.org/abs/2106.06801.
[106] Pham DD, Dovletov G, Pauli J. Liver segmentation in ct with mri data: Zero-shot domain adaptation by contour extraction and shape priors. In: 2020 IEEE 17th international symposium on biomedical imaging (ISBI); 2020. p. 1538–42. https://doi.org/10.1109/ISBI45749.2020.9098615.
[107] Prasad PJR, Elle OJ, Lindseth F, Albregtsen F, Kumar RP. Modifying U-Net for small dataset: a simplified U-Net version for liver parenchyma segmentation. In: Mazurowski MA, Drukker K, editors. Medical imaging 2021: computer-aided diagnosis. International Society for Optics and Photonics. SPIE; 2021. p. 396–405. https://doi.org/10.1117/12.2582179. URL:.
[108] Roth HR, Oda H, Hayashi Y, Oda M, Shimizu N, Fujiwara M, Misawa K, Mori K. Hierarchical 3d fully convolutional networks for multiorgan segmentation. arXiv preprint; 2017. arXiv:1704.06382.
[109] Tang W, Zou D, Yang S, Shi J. Dsl: Automatic liver segmentation with faster r-cnn and deeplab. In: Kůrková V, Manolopoulos Y, Hammer B, Iliadis L, Maglogiannis I, editors. Artificial neural networks and machine learning – ICANN 2018. Cham: Springer International Publishing; 2018. p. 137–47.
[110] Tang X, Jafargholi Rangraz E, Coudyzer W, Bertels J, Robben D, Schramm G, Deckers W, Maleux G, Baete K, Verslype C, et al. Whole liver segmentation based on deep learning and manual adjustment for clinical use in sirt. Eur J Nucl Med Mol Imaging 2020:1–11.
[111] Wang K, Mamidipalli A, Retson T, Bahrami N, Hasenstab K, Blansit K, Bass E, Delgado T, Cunha G, Middleton MS, Loomba R, Neuschwander-Tetri BA, Sirlin CB, Hsiao AA. Automated ct and mri liver segmentation and biometry using a generalized convolutional neural network. Radiology 2019;1:180022. https://doi.org/10.1148/ryai.2019180022. https://doi.org/10.1148/ryai.2019180022.
[112] Xia K, Yin H, Qian P, Jiang Y, Wang S. Liver semantic segmentation algorithm based on improved deep adversarial networks in combination of weighted loss function on abdominal ct images. IEEE Access 2019;7:96349–58.
[113] Xu P, Kim K, Koh J, Wu D, Lee Y, Tak W, Liu H, Li Q. Efficient knowledge distillation for liver ct segmentation using growing assistant network. Phys Med Biol 2021;66. https://doi.org/10.1088/1361-6560/ac3935.
[114] Yang D, Xu D, Zhou SK, Georgescu B, Chen M, Grbic S, Metaxas D, Comaniciu D. Automatic liver segmentation using an adversarial image-to-image network. In: International conference on medical image computing and computer-assisted intervention. Springer; 2017. p. 507–15.
[115] Yang J, Dvornek NC, Zhang F, Chapiro J, Lin M, Duncan JS. Unsupervised domain adaptation via disentangled representations: application to cross-modality liver segmentation. arXiv:1907.13590; 2019. abs/1802.02182.
[116] Yang J, Dvornek NC, Zhang F, Zhuang J, Chapiro J, Lin M, Duncan JS. Domain-agnostic learning with anatomy-consistent embedding for cross-modality liver segmentation. In: 2019 IEEE/CVF international conference on computer vision workshop (ICCVW); 2019. p. 323–31. https://doi.org/10.1109/ICCVW.2019.00043.
[117] You C, Yang J, Chapiro J, Duncan JS. Unsupervised wasserstein distance guided domain adaptation for 3d multi-domain liver segmentation. arXiv:2009.02831; 2020.
[118] Zhou B, Augenfeld Z, Chapiro J, Zhou SK, Liu C, Duncan J. Anatomy-guided multimodal registration by learning segmentation without ground truth: application to intraprocedural cbct/mr liver segmentation and registration. Med Image Anal 2021;71:102041. https://doi.org/10.1016/j.media.2021.102041.
[119] Bellver M, Maninis K, Pont-Tuset J, Girói Nieto X, Torres J, Gool LV. Detection-aided liver lesion segmentation using deep learning. CoRR; 2017.
[120] Ben-Cohen A, Diamant I, Klang E, Amitai M, Greenspan H. Fully convolutional network for liver segmentation and lesions detection. In: Deep learning and data labeling for medical applications. Springer; 2016. p. 77–85.
[121] Bi L, Kim J, Kumar A, Feng D. Automatic liver lesion detection using cascaded deep residual networks. URL: CoRR; 2017.
[122] Bi L, Kim J, Kumar A, Fulham M, Feng D. Stacked fully convolutional networks with multi-channel learning: application to medical image segmentation. Vis Comput 2017;33:1061–71.
[123] Chlebus G, Meine H, Moltz JH, Schenk A. Neural network-based automatic liver tumor segmentation with random forest-based candidate filtering. URL: CoRR; 2017.
[124] Chlebus G, Meine H, Abolmaali N, Schenk A. Automatic liver and tumor segmentation in late-phase mri using fully convolutional neural networks. Proc CURAC 2018:195–200.
[125] Christ PF, Elshaer MEA, Ettlinger F, Tatavarty S, Bickel M, Bilic P, Rempfler M, Armbruster M, Hofmann F, D?Anastasi M. Automatic liver and lesion segmentation in ct using cascaded fully convolutional neural networks and 3d conditional random fields. In: International conference on medical image computing and computer-assisted intervention. Springer; 2016. p. 415–23.
[126] Christ PF, Ettlinger F, Grün F, Elshaer MEA, Lipková J, Schlecht S, Ahmaddy F, Tatavarty S, Bickel M, Bilic P, Rempfler M, Hofmann F, D'Anastasi M, Ahmadi S, Kaissis G, Holch J, Sommer WH, Braren R, Heinemann V, Menze BH. Automatic liver and tumor segmentation of CT and MRI volumes using cascaded fully convolutional neural networks. CoRR; 2017. abs/1702.05970.
[127] Han X. Automatic liver lesion segmentation using A deep convolutional neural network method. CoRR; 2017.
[128] Hoogi A, Lambert JW, Zheng Y, Comaniciu D, Rubin DL. A fully-automated pipeline for detection and segmentation of liver lesions and pathological lymph nodes. CoRR; 2017. abs/1703.06418.
[129] Jiang H, Shi T, Bai Z, Huang L. Ahcnet: an application of attention mechanism and hybrid connection for liver tumor segmentation in ct volumes. IEEE Access 2019. https://doi.org/10.1109/ACCESS.2019.2899608. PP, 1–1.
[130] Kaluva KC, Khened M, Kori A, Krishnamurthi G. 2d-densely connected convolution neural networks for automatic liver and tumor segmentation. CoRR; 2018. abs/1802.02182.
[131] Li W, Jia F, Hu Q. Automatic segmentation of liver tumor in ct images with deep convolutional neural networks. J. Comput. Commun. 2015;3:146.
[132] Li X, Chen H, Qi X, Dou Q, Fu C, Heng P. H-denseunet: Hybrid densely connected unet for liver and liver tumor segmentation from CT volumes. CoRR; 2017. abs/1709.07330.
[133] Sun C, Guo S, Zhang H, Li J, Chen M, Ma S, Jin L, Liu X, Li X, Qian X. Automatic segmentation of liver tumors from multiphase contrast-enhanced ct images based on fcns. Artif Intell Med 2017;83:58–66.
[134] Tian J, Li C, Shi Z, Xu F. A diagnostic report generator from ct volumes on liver tumor with semi-supervised attention mechanism. In: Frangi AF, Schnabel JA, Davatzikos C, Alberola-López C, Fichtinger G, editors. Medical image computing and computer assisted intervention – MICCAI 2018. Cham: Springer International Publishing; 2018. p. 702–10.
[135] Vivanti R, Ephrat A, Joskowicz L, Lev-Cohain N, Karaaslan O, Sosna J. Automatic liver tumor segmentation in follow-up ct scans: preliminary method and results. In: Proc. patch-based methods in medical image processing workshop; 2015. p. 54–61. https://doi.org/10.1007/978-3-319-28194-0_7.
[136] Vivanti R, Szeskin A, Lev-Cohain N, Sosna J, Joskowicz L. Automatic detection of new tumors and tumor burden evaluation in longitudinal liver ct scan studies. Int J Comput Assist Radiol Surg 2017;12:1945–57.
[137] Vorontsov E, Chartrand G, Tang A, Pal C, Kadoury S. Liver lesion segmentation informed by joint liver segmentation. CoRR; 2017. abs/1707.07734.
[138] Zheng S, Fang B, Li L, Gao M, Wang Y, Peng K. Automatic liver lesion segmentation in ct combining fully convolutional networks and non-negative matrix factorization. In: Imaging for patient-customized simulations and systems for point-of-care ultrasound. Springer; 2017. p. 44–51.
[139] Huang Q, Sun J, Ding H, Wang X, Wang G. Robust liver vessel extraction using 3d u-net with variant dice loss function. Comput Biol Med 2018;101. https://doi.org/10.1016/j.compbiomed.2018.08.018.
[140] Ibragimov B, Toesca D, Chang D, Koong A, Xing L. Combining deep learning with anatomical analysis for segmentation of the portal vein for liver sbrt planning. Phys Med Biol 2017;62:8943.
[141] Kitrungrotsakul T, Han XH, Iwamoto Y, Foruzan AH, Lin L, Chen YW. Robust hepatic vessel segmentation using multi deep convolution network. In: Medical imaging 2017: biomedical applications in molecular, structural, and functional imaging. International Society for Optics and Photonics; 2017. p. 1013711.
[142] Mishra D, Chaudhury S, Sarkar M, Soin AS. Ultrasound image segmentation: a deeply supervised network with attention to boundaries. IEEE Trans Biomed Eng 2018;66:1637–48.
[143] Mishra D, Chaudhury S, Sarkar M, Manohar S, Soin AS. Segmentation of vascular regions in ultrasound images: a deep learning approach. In: 2018 IEEE international symposium on circuits and systems (ISCAS). IEEE; 2018. p. 1–5.
[144] Survarachakan S, Pelanis E, Khan ZA, Kumar RP, Edwin B, Lindseth F. Effects of enhancement on deep learning based hepatic vessel segmentation. Electronics 2021:10. https://doi.org/10.3390/electronics10101165. PP, 1–1, https://www.mdpi.com/2079-9292/10/10/1165.
[145] Thomson BR, Nijkamp J, Ivashchenko O, van der Heijden F, Smit JN, Kok NF, Kuhlmann KF, Ruers TJ, Fusaglia M. Hepatic vessel segmentation using a reduced filter 3d u-net in ultrasound imaging. arXiv preprint; 2019.
[146] Yan Q, Wang B, Zhang W, Luo C, Xu W, Xu Z, Zhang Y, Shi Q, Zhang L, You Z. Attention-guided deep neural network with multiscale feature fusion for liver vessel segmentation. IEEE J Biomed Health Inform 2021;25:2629–42.
[147] Yu W, Fang B, Liu Y, Gao M, Zheng S, Wang Y. Liver vessels segmentation based on 3d residual u-net. In: 2019 IEEE international conference on image processing (ICIP). IEEE; 2019. p. 250–4.
[148] Ben-Cohen A, Klang E, Amitai MM, Goldberger J, Greenspan H. Anatomical data augmentation for CNN based pixel-wise classification. CoRR; 2018. abs/1801.02261.
[149] Căleanu CD, Sîrbu CL, Simion G. Deep neural architectures for contrast enhanced ultrasound (ceus) focal liver lesions automated diagnosis. Sensors 2021:21. https://doi.org/10.3390/s21124126. abs/1702.05970, https://www.mdpi.com/1424-8220/21/12/4126.
[150] Liang D, Lin L, Hu H, Zhang Q, Chen Q, Lwamoto Y, Han X, Chen YW, Fichtinger G. Combining convolutional and recurrent neural networks for classification of focal liver lesions in multi-phase ct images. In: Frangi AF, Schnabel JA, Davatzikos C, Alberola-López C, editors. Medical Image Computing and Computer Assisted Intervention – MICCAI 2018. Cham: Springer International Publishing; 2018. p. 666–75.
[151] Liang D, Lin L, Hu H, Zhang Q, Chen Q, Lwamoto Y, Han X, Chen YW. Residual convolutional neural networks with global and local pathways for classification of

focal liver lesions. In: Geng X, Kang BH, editors. PRICAI 2018: Trends in Artificial Intelligence. Cham: Springer International Publishing; 2018. p. 617–28.
[152] Marya NB, Powers PD, Fujii-Lau L, Dayyeh BKA, Gleeson FC, Chen S, Long Z, Hough DM, Chandrasekhara V, Iyer PG, et al. Application of artificial intelligence using a novel eus-based convolutional neural network model to identify and distinguish benign and malignant hepatic masses. Gastrointest Endosc 2021;93:1121–30.
[153] Meng D, Zhang L, Cao G, Cao W, Zhang G, Hu B. Liver fibrosis classification based on transfer learning and fcnet for ultrasound images. IEEE Access 2017;5:5804–10.
[154] Pan F, Huang Q, Li X. Classification of liver tumors with ceus based on 3d-cnn. In: 2019 IEEE 4th international conference on advanced robotics and mechatronics (ICARM); 2019. p. 845–9. https://doi.org/10.1109/ICARM.2019.8834190.
[155] Romero FP, Diler A, Bisson-Gregoire G, Turcotte S, Lapointe R, Vandenbroucke-Menu F, Tang A, Kadoury S. End-to-end discriminative deep network for liver lesion classification. CoRR; 2019. abs/1901.09483. arXiv:1901.09483.
[156] Schmauch B, Herent P, Jehanno P, Dehaene O, Saillard C, Aubé C, Luciani A, Lassau N, Jégou S. Diagnosis of focal liver lesions from ultrasound using deep learning. Diagn Interv Imaging 2019;100:227–33.
[157] Sîrbu CL, Simion G, Căleanu CD. Deep cnn for contrast-enhanced ultrasound focal liver lesions diagnosis. In: 2020 international symposium on electronics and telecommunications (ISETC); 2020. p. 1–4. https://doi.org/10.1109/ISETC50328.2020.9301116.
[158] Trivizakis E, Manikis GC, Nikiforaki K, Drevelegas K, Constantinides M, Drevelegas A, Marias K. Extending 2-d convolutional neural networks to 3-d for advancing deep learning cancer classification with application to mri liver tumor differentiation. IEEE J Biomed Health Inform 2019;23:923–30. https://doi.org/10.1109/JBHI.2018.2886276.
[159] Wu K, Chen X, Ding M. Deep learning based classification of focal liver lesions with contrast-enhanced ultrasound. Optik 2014;125:4057–63.
[160] Yasaka K, Akai H, Abe O, Kiryu S. Deep learning with convolutional neural network for differentiation of liver masses at dynamic contrast-enhanced ct: a preliminary study. Radiology 2017;286:170706. https://doi.org/10.1148/radiol.2017170706.
[161] Zhang F, Yang J, Nezami N, Laage-gaupp F, Chapiro J, De Lin M, Duncan J. Liver tissue classification using an auto-context-based deep neural network with a multi-phase training framework. In: Bai W, Sanroma G, Wu G, Munsell BC, Zhan Y, Coupé P, editors. Patch-based techniques in medical imaging. Cham: Springer International Publishing; 2018. p. 59–66.
[162] Bousabarah K, Letzen B, Tefera J, Savic L, Schobert I, Schlachter T, Staib L, Kocher M, Chapiro J, Lin M. Automated detection and delineation of hepatocellular carcinoma on multiphasic contrastenhanced mri using deep learning. Abdom Radiol 2021;46. https://doi.org/10.1007/s00261-020-02604-5.
[163] Frid-Adar M, Diamant I, Klang E, Amitai M, Goldberger J, Greenspan H. Modeling the intra-class variability for liver lesion detection using a multi-class patch-based cnn. In: International workshop on patch-based techniques in medical imaging. Springer; 2017. p. 129–37.
[164] Jansen MJ, Kuijf HJ, Niekel M, Veldhuis WB, Wessels FJ, Viergever MA, Pluim JP. Liver segmentation and metastases detection in mr images using convolutional neural networks. J Med Imaging 2019;6:044003.
[165] Lee G, Kim J, Lee JG, Ahn G, Park SH, Kim SY, Kim KW, Lee SS, Kim N. Automatic hepatocellular carcinoma lesion detection with dynamic enhancement characteristic from multi-phase CT images. In: International forum on medical imaging in Asia 2019; 2019. p. 1105016. https://doi.org/10.1117/12.2521021.
[166] Wang Z. Triplanar convolutional neural network for automatic liver and tumor image segmentation. Int J Performability Eng 2018;14. https://doi.org/10.23940/ijpe.18.12.p24.31513158.
[167] Guan H, Liu M. Domain adaptation for medical image analysis: a survey. arXiv:2102.09508; 2021.
[168] Long J, Shelhamer E, Darrell T. Fully convolutional networks for semantic segmentation. CoRR; 2014. abs/1411.4038. arXiv:1411.4038.
[169] Huang G, Liu Z, Weinberger KQ. Densely connected convolutional networks. CoRR; 2016. abs/1709.07330.
[170] He K, Zhang X, Ren S, Sun J. Deep residual learning for image recognition. CoRR; 2015. abs/1512.03385. arXiv:1512.03385.
[171] Çiçek Ö, Abdulkadir A, Lienkamp SS, Brox T, Ronneberger O. 3d u-net: learning dense volumetric segmentation from sparse annotation. CoRR; 2016. arXiv:1704.06382.
[172] Erickson BJ, Kirk S, Lee Y, Bathe O, Kearns M, Gerdes C, Lemmerman J. Radiology data from the cancer genome atlas liver hepatocellular carcinoma [tcga-lihc] collection. Cancer Imaging Arch 2016.
[173] Ronneberger O, Fischer P, Brox T. U-net: convolutional networks for biomedical image segmentation. CoRR; 2015. abs/1505.04597. arXiv:1505.04597.
[174] Russakovsky O, Deng J, Su H, Krause J, Satheesh S, Ma S, Huang Z, Karpathy A, Khosla A, Bernstein M, Berg AC, Fei-Fei L. ImageNet large scale visual recognition challenge. Int J Comput Vis 2015;115:211–52. https://doi.org/10.1007/s11263-015-0816-y.
[175] He K, Gkioxari G, Dollár P, Girshick RB. Mask R-CNN. CoRR; 2017. abs/1703.06870. arXiv:1703.06870.
[176] Simonyan K, Zisserman A. Very deep convolutional networks for large-scale image recognition. CoRR; 2014.
[177] Milletari F, Navab N, Ahmadi S. V-net: fully convolutional neural networks for volumetric medical image segmentation. CoRR; 2016. abs/1606.04797. arXiv:1606.04797.
[178] Sudlow C, Gallacher J, Allen N, Beral V, Burton P, Danesh J, Downey P, Elliott P, Green J, Landray M, Liu B, Matthews P, Ong G, Pell J, Silman A, Young A, Sprosen T, Peakman T, Collins R. Uk biobank: an open access resource for identifying the causes of a wide range of complex diseases of middle and old age. PLoS Med 2015;12:1–10. https://doi.org/10.1371/journal.pmed.1001779.
[179] Xia X, Kulis B. W-net: a deep model for fully unsupervised image segmentation. abs/1711.08506. URL: CoRR; 2017. arXiv:1711.08506, http://arxiv.org/abs/1711.08506.
[180] Hamarneh G, Jassi P. Vascusynth: simulating vascular trees for generating volumetric image data with ground truth segmentation and tree analysis. Comput Med Imaging Graph 2010;34:605–16. https://doi.org/10.1016/j.compmedimag.2010.06.002.
[181] Jassi P, Hamarneh G. Vascusynth: vascular tree synthesis software. Insight J 2011;1–12. 10380/3260.
[182] Krizhevsky A, Sutskever I, Hinton GE. Imagenet classification with deep convolutional neural networks. Neural Inf Proces Syst 2012:25. https://doi.org/10.1145/3065386.
[183] Chen T, Kornblith S, Norouzi M, Hinton G. A simple framework for contrastive learning of visual representations. URL:. In: III HD, Singh A, editors. Proceedings of the 37th international conference on machine learning, PMLR; 2020. p. 1597–607. http://proceedings.mlr.press/v119/chen20j.html.
[184] Lassau N, Estienne T, de Vomecourt P, Azoulay M, Cagnol J, Garcia G, Majer M, Jehanno E, Renard-Penna R, Balleyguier C, Bidault F, Caramella C, Jacques T, Dubrulle F, Behr J, Poussange N, Bocquet J, Montagne S, Cornelis F, Faruch M, Bresson B, Brunelle S, Jalaguier-Coudray A, Amoretti N, Blum A, Paisant A, Herreros V, Rouviere O, Si-Mohamed S, Di Marco L, Hauger O, Garetier M, Pigneur F, BergÃsre A, Cyteval C, Fournier L, Malhaire C, Drape JL, Poncelet E, Bordonne C, Cauliez H, Budzik JF, Boisserie M, Willaume T, MolīÃsre S, Peyron Faure N, Caius Giurca S, Juhan V, Caramella T, Perrey A, Desmots F, Faivre-Pierre M, Abitbol M, Lotte R, Istrati D, Guenoun D, Luciani A, Zins M, Meder JF, Cotten A. Five simultaneous artificial intelligence data challenges on ultrasound, ct, and mri. Diagn Interv Imaging 2019;100:199–209. https://doi.org/10.1016/j.diii.2019.02.001. https://www.sciencedirect.com/science/article/pii/S2211568419300294.
[185] Clark K, Vendt B, Smith K, Freymann J, Kirby J, Koppel P, Moore S, Phillips S, Maffitt D, Pringle M, Tarbox L, Prior F. The cancer imaging archive (tcia): maintaining and operating a public information repository. J Digit Imaging 2013;26:1045–57. https://doi.org/10.1007/s10278-013-9622-7. copyright: Copyright 2013 Elsevier B.V., All rights reserved.
[186] Prasad PJR, Survarachakan S, Khan ZA, Lindseth F, Elle OJ, Albregtsen F, Kumar RP. Numerical evaluation on parametric choices influencing segmentation results in radiology images—a multi-dataset study. Electronics 2021;10. https://doi.org/10.3390/electronics10040431. https://www.mdpi.com/2079-9292/10/4/431.